
Excitons

Contents

1	Optical Transitions of Free Excitons	486
1.1	Frenkel Excitons	488
1.2	Wannier–Mott Excitons	491
1.3	Exciton–Polaritons	504
1.4	Trions and Biexcitons in Bulk Crystals	509
2	Excitons in Low-Dimensional Semiconductors	511
2.1	Excitons in Quantum Wells	511
2.2	Biexcitons and Trions in Quantum Wells	515
2.3	Excitons in Quantum Wires and Quantum Dots	516
3	Summary	520
	References	521

Abstract

Optical band-to-band absorption can produce an electron and a hole in close proximity which attract each other via Coulomb interaction and can form a hydrogen-like bond state, the exciton. The spectrum of free Wannier–Mott excitons in bulk crystals is described by a Rydberg series with an effective Rydberg constant given by the reduced effective mass and the dielectric constant. A small dielectric constant and large effective mass yield a localized Frenkel exciton resembling an excited atomic state. Excitons increase the absorption slightly below the band edge significantly. The interaction of photons and excitons creates a mixed state, the exciton–polariton, with photon-like and exciton-like dispersion branches. An exciton can bind another exciton or carriers to form molecules or higher associates of excitons. Free charged excitons (trions) and biexcitons have a small binding energy with respect to the exciton state. The binding energy of all excitonic quasiparticles is significantly enhanced

in low-dimensional semiconductors. Basic features of confined excitons with strongest transitions between electron and hole states of equal principal quantum numbers remain similar. The analysis of exciton spectra provides valuable information about the electronic structure of the semiconductor.

Keywords

Band-to-band absorption · Biexciton · Binding energy · Bound exciton · Confined exciton · Coulomb interaction · Dielectric constant · Effective mass · Exciton complex · Exciton spectra · Excitonic quasiparticles · Exciton–polariton · Free exciton · Frenkel exciton · Indirect-gap exciton · Quasi-hydrogen states · Rydberg constant · Rydberg series · Trion · Wannier-Mott exciton

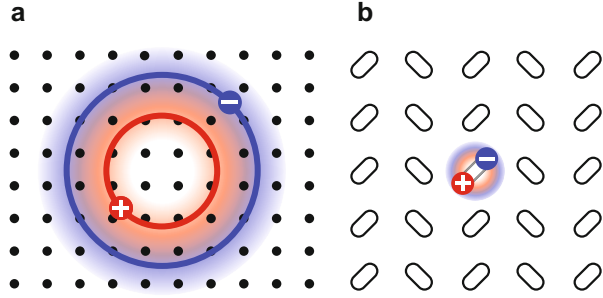
1 Optical Transitions of Free Excitons

The transitions discussed in the previous chapters considered electron–hole pair generation by the absorption of a photon with bandgap energy E_g and neglected the Coulomb attraction between the created electron and hole. With photons of $h\nu \cong E_g$, both electron and hole do not have enough kinetic energy at low temperatures to separate. They form a bound state. This state can be modeled by an electron and a hole, circling each other much like the electron and proton in a hydrogen atom, except that they have almost the same mass¹; hence, in a semiclassical model, their center of rotation lies closer to the middle on their interconnecting axis (Fig. 1). This bound state is called an *exciton*. These excitons have a significant effect on the optical absorption close to the absorption edge. There are various kinds of excitons. *Free excitons*, the main topic of Sect. 1, are free to move in the crystal; further classification distinguishes the degree of localization and free excitons in direct or indirect semiconductors. *Confined excitons* experience spatial restrictions by heterojunctions in low-dimensional semiconductors and are discussed in Sect. 2. *Bound excitons* are excitons trapped in the potential of a defect, e.g., an impurity atom, when the interaction to the defect becomes larger than their thermal energy; their analysis requires a knowledge of the specific defect and is considered in ▶ Sect. 2 of chapter “Shallow-Level Centers”. Furthermore, an exciton may be (weakly) bound to a free carrier or another exciton, forming a charged exciton (a *trion*) or an *exciton complex*. These states are discussed in Sects. 1.4, 2.2, and 2.3.

The Hamiltonian to describe a free exciton can be approximated as

¹This causes the breakdown of the adiabatic approximation. The error in this approximation is on the order of the fourth root of the mass ratio. For hydrogen this is $(m_n/M_H)^{1/4} \cong 10\%$ and is usually acceptable. For excitons, however, the error is on the order of 1 and is no longer acceptable. This is relevant for the estimation of exciton molecule formation discussed in Sect. 1.4.

Fig. 1 (a) Exciton with a large radius extending over many lattice constants and a center of mass slightly shifted toward the heavier hole (Wannier–Mott exciton). (b) Exciton with a small radius localized at a molecule in an organic crystal or an atom in an organic crystal (Frenkel exciton)



$$H = H_0 + U, \quad U = -\frac{e^2}{4\pi\epsilon\epsilon_0|\mathbf{r}_e - \mathbf{r}_h|}, \quad (1)$$

where H_0 is the kinetic energy of the electron–hole pair in the center-of-mass frame (we neglect the center-of-mass kinetic energy) and U describes the Coulomb attraction between the electron and hole, screened by the dielectric constant ϵ . The Schrödinger equation $H\psi = E\psi$ has as eigenvalues a series of quasi-hydrogen states

$$E_{\text{exc}, n} = -R_\infty \frac{\mu}{m_0} \frac{1}{\epsilon^2} \frac{1}{n^2} \quad \text{with} \quad R_\infty = \frac{m_0 e^4}{8\epsilon_0^2 h^2} = 13.6 \text{ eV}, \quad (2)$$

where R_∞ is the Rydberg energy, μ is the reduced exciton mass given by $\mu^{-1} = m_n^{-1} + m_p^{-1}$ for simple parabolic bands, and n as the principal quantum number. The exciton radius is a quasi-hydrogen radius

$$a_{\text{exc}, n} = a_H \frac{\epsilon}{\mu/m_0} n^2 \quad \text{with} \quad a_H = \frac{h^2 \epsilon_0}{\pi m_0 e^2} = 0.529 \text{ \AA}, \quad (3)$$

where a_H is the Bohr radius of the hydrogen atom. For a review, see Bassani and Pastori-Parravicini (1975), Haken (1976), or Singh (1984).

Depending on the reduced exciton mass and dielectric constant, one distinguishes between *Wannier–Mott excitons*, which extend over many lattice constants and are free to move through the lattice, and *Frenkel excitons*, which have a radius comparable to the interatomic distance. Frenkel excitons become localized and resemble an atomic excited state (for more detail, see Singh (1984)). For the large Wannier–Mott excitons, the screening of the Coulomb potential is appropriately described by the static dielectric constant ϵ_{stat} which is used in Eq. 2.

When the lattice interaction is strong, the electron–hole interaction can be described by an *effective* dielectric constant $\epsilon^* = \left(\epsilon_{\text{opt}}^{-1} + \epsilon_{\text{stat}}^{-1} \right)^{-1}$, which provides less shielding. A further reduction of the correlation energy by modifying the

effective dielectric constant was introduced by Haken (1963 – see ► Eq. 96 of chapter “Interaction of Light with Solids”):

$$U = -\frac{e^2}{4\pi\epsilon_0|\mathbf{r}_e - \mathbf{r}_h|} \left\{ \frac{1}{\epsilon_{\text{stat}}} + \frac{1}{2} \left(\frac{1}{\epsilon_{\text{opt}}} - \frac{1}{\epsilon_{\text{stat}}} \right) \left[\exp\left(\frac{r_e}{r_{\text{pe}}}\right) + \exp\left(\frac{r_h}{r_{\text{ph}}}\right) \right] \right\}. \quad (4)$$

Here, r_{pe} and r_{ph} are the electron and hole *polaron* radii², respectively. The radius of the exciton consequently shrinks, and the use of the effective mass becomes questionable. Here, a tight-binding approximation becomes more appropriate to estimate the eigenstates of the exciton, which is now better described as a Frenkel exciton.

For both types of excitons, one obtains eigenstates below the bandgap energy by an amount given by the binding energy of the exciton. In estimating the binding energy, the band structure of valence and conduction bands must be considered, entering into the effective mass and dielectric function. Such structures relate to light- and heavy-hole bands, energy and position in \mathbf{k} of the involved minima of the conduction band, and other features determining band anisotropies. This will be explained in more detail in the following sections. We will first discuss some of the general features of Frenkel and Wannier–Mott excitons.

1.1 Frenkel Excitons

Frenkel excitons (Frenkel 1931 – see also Landau 1933) are observed in ionic crystals with relatively small dielectric constants, large effective masses, and strong coupling with lattice, as well as in organic molecular crystals (see below). These excitons show relatively large binding energies, usually in excess of 0.5 eV, and are also referred to as tight-binding excitons. They cannot be described in a simple hydrogenic model.

1.1.1 Excitons in Alkali Halides

In alkali halides Frenkel excitons with lowest energy are localized at the negatively charged halogen ion, which have lower excitation levels than the positive ions. Figure 2 shows the absorption spectrum of KCl with two relatively narrow Frenkel exciton absorption lines. They relate to the two valence bands at the Γ point that are shifted by spin–orbit splitting. The doublet can be interpreted as excitation of the Cl^- ion representing the valence bands in KCl. This absorption produces tightly bound excitons, but does not produce free electrons or holes; that

²When a quasi-free charge carrier (electron or hole) moves through a crystal with strong lattice polarization, it is surrounded by a polarization cloud. Carrier plus polarization form a *polaron*, a quasiparticle with an increased effective mass (see ► Sect. 1.2 of chapter “Carrier-Transport Equations”).

Fig. 2 Absorption spectrum of KCl at 10 K with two narrow exciton peaks identified as transitions at the Γ point. The hydrogen-like series are due to the Coulomb tail of the potential (After Tomiki 1969)

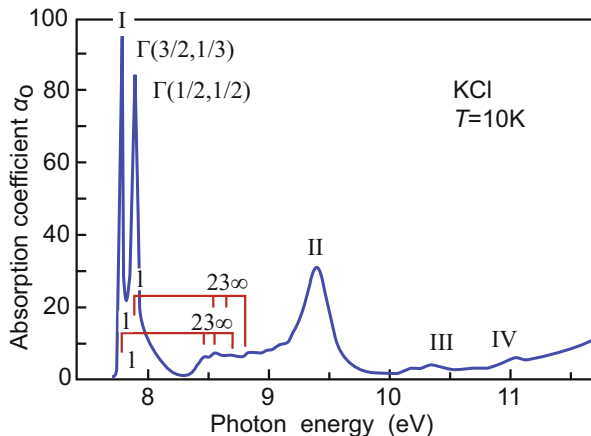


Table 1 Experimental lowest-excitation energies $E_{exc,0}$ of Frenkel excitons for alkali-halide crystals; E_g and E_B denote, respectively, the bandgap energy and the resulting binding energy

Crystal	E_g (eV)	$E_{exc,0}$ (eV)	E_B (eV)
LiF	13.7	12.8	0.9
NaF	11.5	10.7	0.8
NaCl	8.8	7.9	0.9
NaBr	7.1	6.7	0.4
KF	10.8	9.9	0.9
KCl	8.7	7.8	0.9
KBr	7.4	6.7	0.7

is, it does not produce photoconductivity as does an absorption at higher energy. The excited state of the Cl^- is considered the Frenkel exciton (see Kittel 1966). It may move from one Cl^- to the next Cl^- ion by quantum-mechanical exchange. The long-range Coulomb attraction between electron and hole permits additional excited states which have a hydrogen-like character, although with higher binding energy (~ 1 eV) than in typical semiconductors because of a large effective mass and relatively small dielectric constant. An extension of a short-range (tight-binding) potential with a Coulomb tail is observed in a large variety of lattice defects (see chapter ► “Deep-Level Centers”) and provides characteristics mixed between a deep-level and a shallow-level series. It creates a mixture of properties with Frenkel and Wannier–Mott contributions (see Tomiki 1969).

Lowest excitation energies $E_{exc,0}$ of Frenkel excitons in alkali halides are listed in Table 1 (Song and Williams 1993). The large difference to the bandgap energy E_g yields large binding energies $E_B = E_g - E_{exc,0}$, which significantly exceed those of Wannier excitons.

The strength of the exciton absorption substantially exceeds that of the band edge which coincides with the series limit ($n = \infty$). The features to the right of this limit in Fig. 2, labeled with roman numerals, result from excitation into the higher conduction bands.

1.1.2 Excitons in Organic Crystals

Frenkel excitons are observed particularly in organic molecular crystals, such as in anthracene, naphthalene, benzene, etc., where the binding forces within the molecule (covalent) are large compared to the binding forces between the molecules (van der Waals interaction, see ► Sect. 1.5 of chapter “The Structure of Semiconductors”). Here, localized excited states within the molecules are favored.

If more than one electron is involved in the excited state, we can distinguish singlet and triplet excited states, while the ground state is always a singlet state (see Fig. 3a). In recombination, the singlet–singlet transition is allowed (it is a luminescent transition), while the triplet–singlet transition is spin forbidden. Consequently, the triplet state has a long lifetime, depending on possible triplet/singlet mixing, and a much weaker luminescence.

Such singlet and triplet excitons are common in organic semiconductors and have been discussed extensively (see Pope and Swenberg 1982). Their importance has also been recognized in inorganic semiconductors in the neighborhood of crystal defects (Cavenett 1984; Davies et al. 1984) and also in layered semiconductors (GaS and GaSe; Cavenett 1980). The luminescence of singlet excitons is employed in organic LED (OLED) devices used to create displays for, e.g., mobile phones or TV screen or for solid-state lighting; for more information, see Shinar (2004) and Kamtekar et al. (2010).

An example of a molecular singlet and triplet Frenkel exciton is shown in Fig. 3. Panel (a) gives the level scheme of organic molecules with an even number of π electrons (i.e., no ions or radicals); the absorption spectrum for tetrachlorobenzene

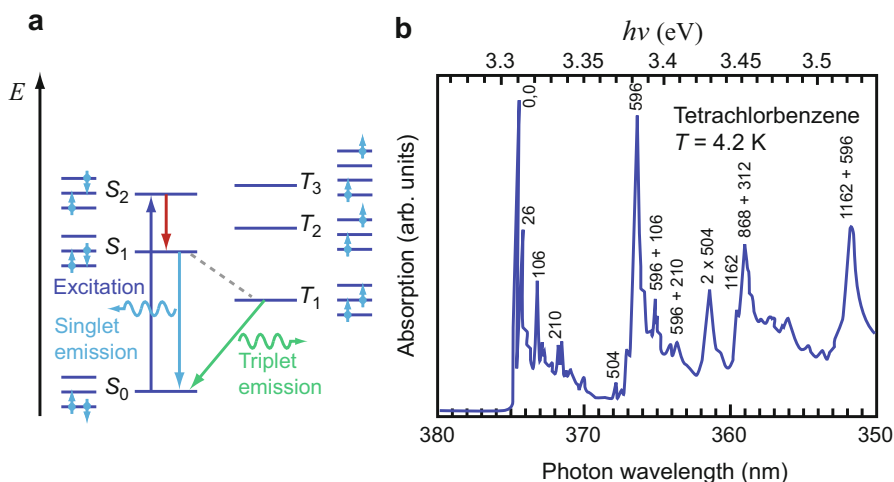


Fig. 3 (a) Singlet/triplet exciton schematics with ground state S_0 , excited singlet states S_1 and S_2 , and triplet states T_1 to T_3 ; occupied spin states are indicated beside the electronic levels. (b) Optical absorption spectrum of singlet–triplet excitons in a tetrachlorobenzene crystal platelet, measured at 4.2 K with unpolarized light; line labels denote energy differences in units of cm^{-1} with respect to the zero-phonon line labeled 0,0 (After George and Morris 1970)

is shown in panel (b). The transition near 375 nm labeled 0,0 refers to the $T_1 \leftarrow S_0$ absorption; transitions at shorter wavelength originate from additional excitations of molecule and lattice vibrations with energies indicated at the lines. When the unit cell contains more than one identical atom or molecule, an additional small splitting of the excited eigenstates occurs. This is referred to as *Davydov splitting* and is observed in molecule crystals but not in isolated molecules.

For the exciton transport, we have to distinguish between triplet and singlet excitons – for a short review, see Knox (1984). For the latter, a dipole–dipole interaction via radiation, i.e., luminescence and reabsorption, contributes to the exciton transport. Such a mechanism is negligible for triplet excitons, which have a longer lifetime and therefore much lower luminescence. For exciton diffusion, see ► Sect. 2 of chapter “Carrier-Transport Equations”.

1.2 Wannier–Mott Excitons

Wannier–Mott excitons are found in most of the typical semiconductors and extend over many lattice constants (see Wannier 1937 and Mott 1938). In the center-of-mass frame, their eigenfunctions, which solve the Schrödinger equation with the Hamiltonian Eq. 1, can be written as the sum of two terms: a translational part $\phi(\mathbf{R})$ describing the motion of the entire exciton as a particle with mass $M = m_n + m_p$ and a rotational part $\phi_n(\mathbf{r})$ related to the rotation of electron and hole about their center of mass:

$$\psi = \phi(\mathbf{R}) + \phi_n(\mathbf{r}). \quad (5)$$

The center-of-mass coordinate \mathbf{R} and the electron–hole separation \mathbf{r} are given by

$$\mathbf{R} = \frac{m_n \mathbf{r}_e + m_p \mathbf{r}_h}{m_n + m_p} \text{ and } \mathbf{r} = \mathbf{r}_e - \mathbf{r}_h. \quad (6)$$

The Schrödinger equation of the translation is

$$-\frac{\hbar^2}{2M} \frac{\partial^2}{\partial \mathbf{R}^2} \phi(\mathbf{R}) = E_K \phi(\mathbf{R}), \quad (7)$$

with the eigenfunctions and eigenvalues determined by the wavevector $\mathbf{K} = \mathbf{k}_e + \mathbf{k}_h$ of the entire exciton:

$$\phi(\mathbf{R}) = e^{i\mathbf{K}\cdot\mathbf{R}}, E_K = \frac{\hbar^2 |\mathbf{K}|^2}{2M}. \quad (8)$$

The rotation is described by

$$\left(-\frac{\hbar^2}{2\mu} \frac{\partial^2}{\partial \mathbf{r}^2} - \frac{e^2}{4\pi\epsilon\epsilon_0 |\mathbf{r}|} \right) \phi_n(\mathbf{r}) = E_n \phi_n(\mathbf{r}), \quad (9)$$

solved by the quasi-hydrogen eigenvalues given in Eq. 2.

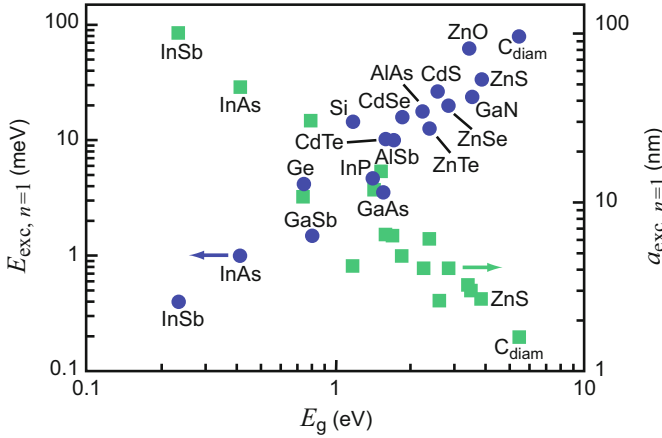


Fig. 4 Exciton binding energy (blue symbols) and ground-state Bohr radius for semiconductors (green symbols) at low temperature. Ordinate and abscissa values are from ▶ Table 2 and ▶ Table 8 of chapter “Bands and Bandgaps in Solids,” respectively

For isotropic parabolic bands, the minimum optical energy needed to excite an electron and to create an exciton is slightly smaller than the bandgap energy:

$$E_{g,exc} = E_g - R_\infty \frac{\mu}{m_0} \frac{1}{\epsilon_{stat}^2} \frac{1}{n^2} + \frac{\hbar^2 K^2}{2(m_n + m_p)} \text{ with } n = 1, 2, \dots ; \quad (10)$$

the second term is the quasi-hydrogen binding energy (Eq. 2) with $\epsilon = \epsilon_{stat}$, and the third term is the kinetic energy due to the center-of-mass motion of the exciton. This term leads to a broadening of optical transitions compared to those of bound and confined excitons. The bandgap energy can be determined from two transitions of the series; e.g., from the 1S and 2S transition energies $E_g = E_{g,exc} + R_\infty^{eff} = \frac{4}{3}(E(2S) - E(1S)) + R_\infty^{eff}$ is concluded, with R_∞^{eff} the effective Rydberg energy (or binding energy $E_{exc,n=1}$) of the exciton. The values of the binding energy $E_{exc,n=1}$ (Eq. 2) and the quasi-hydrogen Bohr radius $a_{exc,n=1}$ (Eq. 3) show a clear trend in the dependence on bandgap energy: Fig. 4 shows the increase of the binding energy and the decrease of the exciton Bohr radius for increasing low-temperature bandgap. For a listing of exciton energies, see Table 2. The Wannier–Mott exciton is mobile and able to diffuse (see chapter ▶ “Carrier-Transport Equations”). Since it has no net charge, it is not influenced in its motion by an electric field³ and does not contribute directly to the electric current.

³It is, however, influenced by the *gradient* of an electric field or by strain; see, e.g., Tamor and Wolfe 1980.

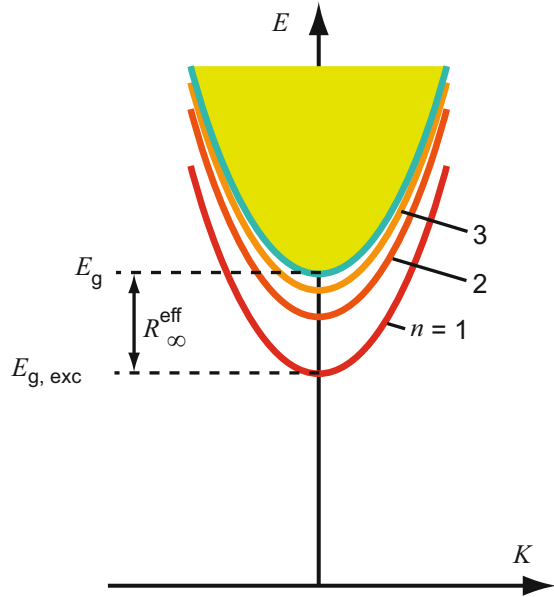
Table 2 Experimental parameters of 1S Wannier–Mott excitons for some semiconductors at low temperature; d and i denote direct and indirect excitons, respectively, and A , B , C excitons with holes from the respective valence bands in wurtzite crystals; T signifies the measurement temperature; 0 refers to extrapolated data

Crystal	d/i	Ground-state energy $E_{g,exc}^{1S}$ (eV)	$T(K)$	Binding energy $E_{exc,n=1}$ (meV)	Bohr radius $a_{exc,n=1}$ (Å)	Reduced mass μ (m_0)
C _{diam}	i	5.409	1.6	80	16	0.191
Si	i	1.1545	1.6	14.7	42	0.145
Ge	i	0.7405	2.1	4.2 ($\pm 3/2$) 3.1 ($\pm 1/2$)	108 143	0.079 0.059
AlN	d	6.025 (A) 6.243 (B) 6.257 (C)	1.7 1.7 1.7	~ 55 (A) ~ 55 (B) ~ 55 (C)		
AlAs	i	2.228	2	18	41	0.134
AlSb	i	1.677	4.2	10	64	0.092
α -GaN	d	3.476 (A) 3.482 (B) 3.499 (C)	4.2 4.2 4.2	24.0 (A) 22.8 (B) 24.5 (C)	31 (A) 33 (B) 31 (C)	0.164 (A) 0.156 (B) 0.168 (C)
β -GaN	d	3.2725		26	32	0.156
GaAs	d	1.5152	2	3.6	155	0.044
GaSb	d	0.8099	2	1.5	306	0.027
InP	d	1.4814	2	4.8	120	0.055
InAs	d	0.4157	4.8	1.0	494	0.016
InSb	d	0.2347	1.7	0.4	1017	0.009
ZnO	d	3.3756 (A) 3.3811 (B) 3.4327 (C)	1.5 1.5 1.5	63 (A) 50 (B) 49 (C)	32 (A) 35 (B) 37 (C)	0.062 (A) 0.057 (B) 0.054 (C)
α -ZnS	d	3.8069	0	34.2	27	0.106
ZnSe	d	2.8052	0	19.9	41	0.119
ZnTe	d	2.3816	0	12.7	62	0.078
α -CdS	d	2.5529 (A) 2.5676 (B)	1.6 1.8	27 (A) 31 (B) 30 (C)	26 25 25	0.197 (A) 0.204 (B) 0.211 (C)
CdSe	d	1.8265 (A) 1.8503 (B)	0 0	15.7 (A) 16.7 (B)	48 45	0.106 (A) 0.112 (B)
CdTe	d	1.595	4.8	10.5	65	0.085
Cu ₂ O	d	2.1472 ($n = 2$)	1.2	98 ($n \geq 2$)	11	0.407

The ionization energy⁴ of these excitons in typical semiconductors is on the order of 10 meV (Table 2 and Thomas and Timofeev 1980); hence, the thermal energy kT at room temperature (26 meV) is sufficient to dissociate most of them.

⁴The ionization energy is also referred to as binding energy or Rydberg energy.

Fig. 5 Band model with exciton levels that result in a hydrogen-like line spectrum for direct-gap semiconductors. The shaded area above E_g indicates unbound continuum states



The principal quantum number n defines S states ($l = 0$) which contribute to electric dipole transitions in direct-gap semiconductors with allowed transitions, while P states ($l = 1$) contribute to dipole-forbidden transitions (see triplet excitons in previous section). With introduction of symmetry-breaking effects, such as external fields, external stresses, or those in the neighborhood of crystal defects (Gislason et al. 1982), and moving slightly away from $\mathbf{k} = 0$, the other quantum numbers, l and m , need to be considered. This results in a more complex line spectrum. Exciton transitions with $n \rightarrow \infty$ merge into the edge of the band continuum (Fig. 5).

At low temperatures, excitons have a major influence on the optical absorption spectrum. This can be seen from the matrix elements M_{cv} for transitions from near the top of the valence band to the vicinity of the bottom of the conduction band. When considering exciton formation, the band-to-band transition matrix elements (e.g., ► Eq. 21 of chapter “Band-to-Band Transitions”) are modified by multiplication with the eigenfunction of the exciton $\phi_n(\mathbf{r})$ as discussed in the following.

1.2.1 Direct-Gap Excitons

For an excitonic single-photon absorption at the Γ point in a direct-bandgap material, the matrix element is given by

$$M_{cv}^{(exc)} = M_{cv} \phi_n(0), \quad (11)$$

with M_{cv} given by ► Eq. 21 of chapter “Band-to-Band Transitions”. The strength of the absorption is proportional to the square of the matrix element, which yields

$$\alpha_{o,vc,exc} = \alpha_{o,vc} |\phi_n(0)|^2, \quad (12)$$

where $\alpha_{o,vc}$ is the valence-to-conduction band optical absorption coefficient neglecting excitons. In the case of isotropic parabolic bands, the eigenfunction of the n^{th} exciton state is related to the ground state with $n = 1$ by

$$|\phi_n(0)|^2 = n^{-3} |\phi_1(0)|^2. \quad (13)$$

For exciton states⁵ below the bandgap, it follows

$$|\phi_n(0)|_{h\nu < E_g}^2 = \begin{cases} \frac{1}{a_{qH}^3 n^3} & \text{allowed} \\ \frac{n^2 - 1}{\pi a_{qH}^5 n^5} & \text{forbidden} \end{cases} \quad (14)$$

for the indicated type of transitions (► Sects. 1.3 and ► 2.2 of chapter “Band-to-Band Transitions”) and with the quasi-hydrogen radius $a_{qH} = a_H \varepsilon_{\text{stat}} m_0 / \mu = a_{\text{exc},n=1}$ for $\varepsilon = \varepsilon_{\text{stat}}$. For higher excited states, the line intensity decreases proportional to n^{-3} or $n^{-5}(n^2 - 1)$ for allowed or forbidden transitions. The optical absorption per center is spread over a large volume element of radius $a_{qH} \cdot n^2$; therefore, the corresponding matrix element is reduced accordingly. The spacing of the absorption lines is given by

$$E_{g,exc}^{(\text{dir})} = E_g - E_{\text{exc},n}; \quad (15)$$

E_g is also the limit of the line series (Fig. 5). Hence, we expect one strong line for the ground state in absorption, followed by much weaker lines for the excited states which converge at the absorption edge (see Fig. 7).

Electric dipole-forbidden (1S) transitions⁶ are observed in only a few semiconductors. Most extensively investigated is Cu_2O with d -like valence bands, which has two series of hydrogen-like levels – the yellow (superscript y) and the green (superscript g) series from the Γ_7 and Γ_8 valence bands, respectively. The observed level spectra are given in Fig. 6, with

⁵ $\phi_n(0) \neq 0$ applies only for S states.

⁶Strictly, such transitions cannot occur at $\mathbf{k} = 0$; however, a slight shift because of the finite momentum of the photon permits the optical transition to occur because of a weak electric quadrupole coupling (Elliott 1961). Such transitions can also be observed under a high electric field using modulation spectroscopy (Washington et al. 1977). Dipole-forbidden transitions are easily detected with Raman scattering (Sect. 1.3) or two-photon absorption (for Cu_2O , see Uihlein et al. 1981), which follow different selection rules.

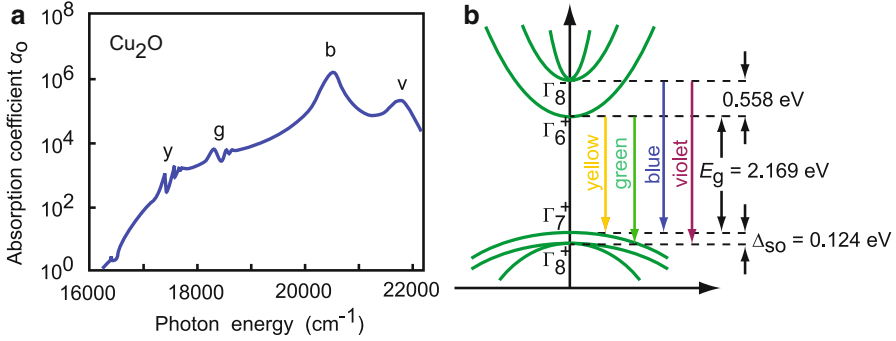


Fig. 6 (a) Absorption spectrum and (b) band structure near the Γ point of Cu_2O with strong dipole-allowed (*blue* and *violet*) and weak forbidden (*yellow* and *green*) transitions. The absorption below the *yellow* series corresponds to indirect transitions to the $1S$ exciton via phonon coupling

$$E_n^{(y)} = (2.1661 - 0.0971/n^2) \text{ eV} \text{ and } E_n^{(g)} = (2.2975 - 0.1565/n^2) \text{ eV} \quad (16)$$

for the P levels of these two series. According to the second case of Eq. 14, the series starts with $n = 2$ (Fig. 7b) and is observed up to $n = 25$ in pure Cu_2O crystals⁷ (Kazimierczuk et al. 2014). In addition, there are two dipole-allowed excitons in the blue and violet range of the spectrum from the two valence bands into the higher conduction band Γ_{12} (Compaan 1975). Figure 7b shows that with sufficient perturbation by an electric field, the electric dipole selection-rule is broken, and the S transitions are also observed in the yellow (and also in the green) series. Another material showing forbidden exciton spectra is SnO_2 .

In contrast to the strongly absorbing Frenkel exciton with a highly localized electron–hole wavefunction in the ground state, the intensity of the Wannier–Mott exciton lines is reduced by $(a/a_{\text{qH}})^3$: the larger the quasi-hydrogen radius a_{qH} is compared to that of the corresponding atomic eigenfunction a , the weaker is the corresponding absorption line (see Fig. 7b and Kazimierczuk et al. 2014).

For $h\nu > E_g$ near the band edge, the absorption is substantially increased due to the effect of the Coulomb interaction. With exciton contribution, a semiconductor with a *direct* bandgap between spherical parabolic bands has an increased absorption given by (for details, see Bassani and Pastori-Parravicini 1975)

$$\alpha_{\text{o,vc,exc}}^{(\text{dir})} = \begin{cases} \gamma_e \frac{\exp\gamma_e}{\sinh\gamma_e} & \text{allowed} \\ \gamma_e \frac{[1 + (\gamma_e/\pi)^2] \exp\gamma_e}{\sinh\gamma_e} & \text{forbidden} \end{cases}, \text{ with } \gamma_e = \pi \sqrt{\frac{E_{\text{exc},n}}{h\nu - E_g}}. \quad (17)$$

⁷With a correspondingly large exciton Bohr radius of $1.04 \mu\text{m}$ for $n = 25$, compared to $\sim 1 \text{ nm}$ for $n = 1$.

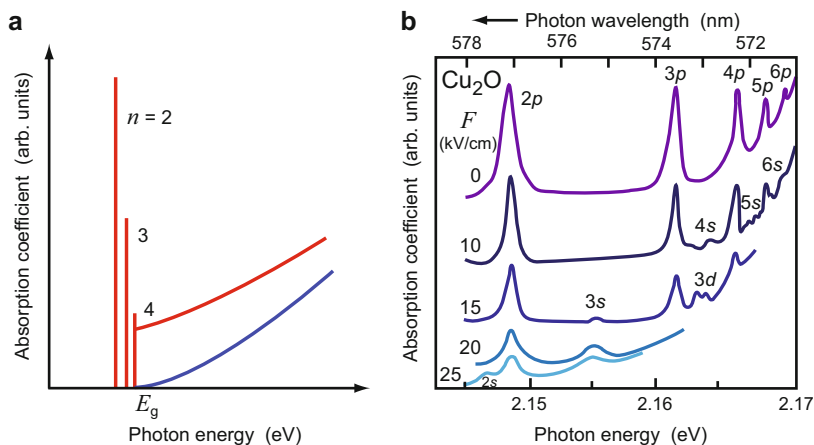


Fig. 7 (a) Direct-bandgap dipole-forbidden transitions including (red curves) and excluding exciton excitation (blue curve). (b) Transitions in Cu_2O at 4 K (After Grosmann 1963)

The Coulomb interaction of the electron and hole influences the relative motion, and the optical absorption in the entire band-edge range is thereby enhanced, as shown in Fig. 8. In semiconductors with large ϵ_{stat} and small reduced mass μ , only the first exciton peak is usually observed: in GaAs the relative distance $E_g - E_{\text{exc}}(\mathbf{K} = 0)$ is only 3.4 meV. Higher absorption lines, which are too closely spaced, are reduced in amplitude and merge with the absorption edge in most direct-gap III–V compounds. Figure 8 shows the pronounced excitonic absorption below the band-edge energy E_g and the onset of continuum absorption above E_g . For an advanced discussion, see Beinikhes and Kogan (1985).

A line spectrum including higher excited states can be observed more easily when it lies adjacent to the reduced absorption of forbidden transitions. It is also easier to observe in materials with a somewhat higher effective mass and lower dielectric constant to obtain a wide enough spacing of these lines. Well-resolved line spectra of higher excited states can be observed when they do not compete with other transitions and are not inhomogeneously broadened by varying lattice environments.

1.2.2 Complexity of Exciton Spectra

The simple hydrogen-like model described above must be modified in real semiconductors because of several contributions (Flohner et al. 1979):

- The anisotropy of effective masses and dielectric constants
- The electron–hole exchange interaction
- The exciton–phonon interaction
- The action of local mechanical stress or electrical fields
- The interaction with magnetic fields

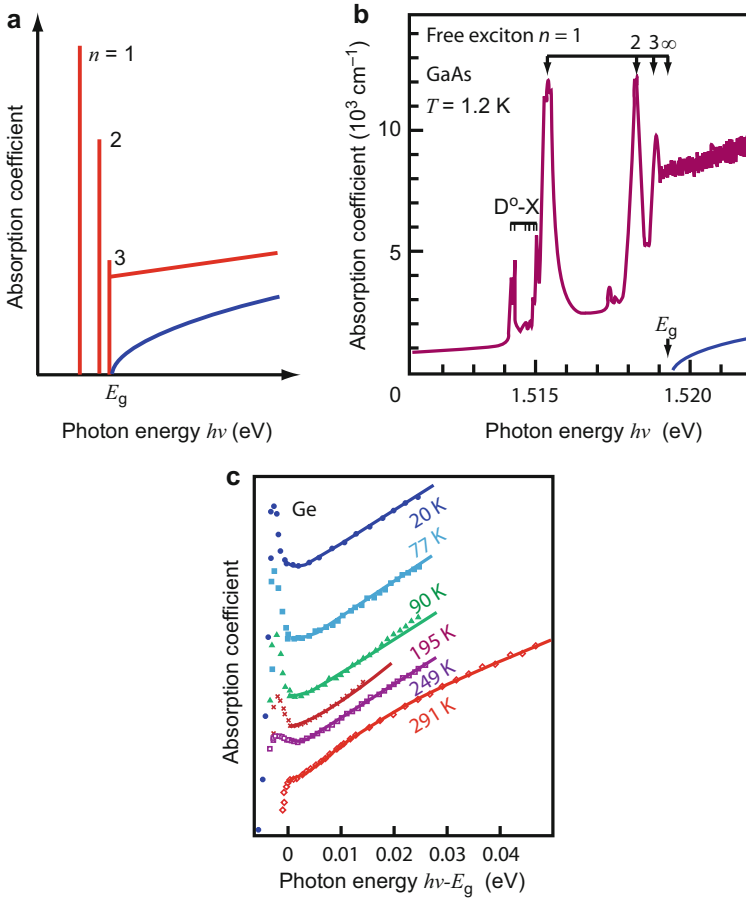
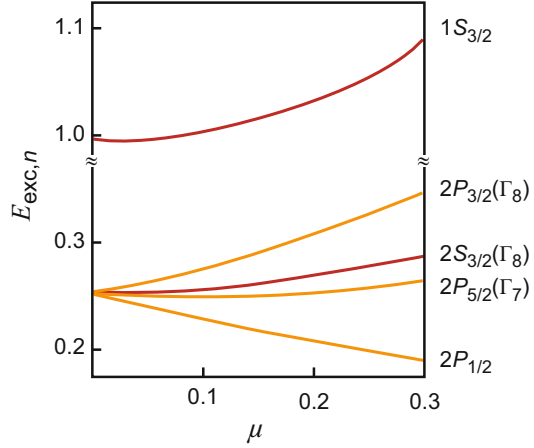


Fig. 8 Direct-bandgap dipole-allowed transitions including exciton excitation (i.e., effects of Coulomb interaction, *red curves* in (a)) and excluding this (*blue curves* in a and b). Examples are (b) for transitions in GaAs (After Weisbuch et al. 2000) and (c) for Ge (After McLean 1963); (c) shows the decrease of absorption at higher temperatures where excitons can no longer exist; measured curves are shifted due to the temperature dependence of the bandgap energy $E_g(T)$

These contributions act on quantum numbers l , m , and s not included in the discussed model; they introduce anisotropies and lift the degeneracy of conduction or valence bands as considered in the following.

The *anisotropy of the effective masses* produces excitons, elongated in the direction in which the mass is smallest. A compression in the direction of the largest effective mass reduces the quasi-hydrogen Bohr radius a_{qH} in this direction by a factor of less than 2 and increases E_{qH} up to a factor of 4 (Shinada and Sugano 1966). The *reduced exciton mass* μ , entering the expression for the exciton energy in Eq. 10, is given by

Fig. 9 Exciton binding energy for *S* and *P* states as a function of the reduced mass (After Baldereschi and Lipari 1973)



$$\frac{1}{\mu} = \frac{2}{3} \frac{1}{\mu_{\perp}} + \frac{1}{3} \frac{\epsilon_{\perp}}{\epsilon_{\parallel}} \frac{1}{\mu_{\parallel}}. \tag{18}$$

The meaning of \perp and \parallel depends on the crystal structure. For instance, in *wurtzite-type semiconductors*, \parallel means parallel to the \mathbf{c} direction. For calculation of the reduced effective mass, we distinguish six effective masses: $m_n^{\perp}, m_n^{\parallel}, m_{pA}^{\perp}, m_{pA}^{\parallel}, m_{pB}^{\perp}, m_{pB}^{\parallel}$ with the *A* and *B* valence bands split by the crystal field with Γ_9 and Γ_7 symmetry, respectively, neglecting the spin–orbit split-off band, the *C* band.

The *lifting of band degeneracies* occurs generally when bands are split by, e. g., intrinsic anisotropy in a crystal or, following the application of mechanical stress, an electric or a magnetic field. The exciton line spectrum can be distinguished with respect to transitions from different valence bands, which result in different exciton line series with different spacings because of a different reduced mass. Taking splitting and warping of the valence bands (► Sects. 1.2.2 and ► 1.2.3 of chapter “Bands and Bandgaps in Solids”) into consideration, one obtains a splitting of the *P*-like exciton states (Baldereschi and Lipari 1973). This is shown in Fig. 9 as a function of the reduced effective mass. The reduced mass μ can in turn be expressed as a function of the Luttinger valence-band parameters:

$$\mu = \frac{6\gamma_3 + 4\gamma_2}{5} \frac{m_n m_0}{m_0 + m_n \gamma_1}. \tag{19}$$

For a review, see Rössler (1979) and Hönerlage et al. (1985).

The *electron–hole exchange interaction* due to the coupling of the electron and hole spins contains a short-range (J_{SR}) and a long-range term (J_{LR}) (also referred to as analytic and nonanalytic contributions), which depend on the wavevector of the exciton motion: $J_{\text{longitudinal}} = J_{SR} + \frac{2}{3}J_{LR}$ and $J_{\text{transversal}} = J_{SR} - \frac{1}{3}J_{LR}$. Thereby the fourfold degenerate $A(n = 1)$ exciton is split into two Γ_6 and Γ_5 exciton states, each twofold degenerate (compare Fig. 10b); the fourfold $B(n = 1)$ exciton splits into the

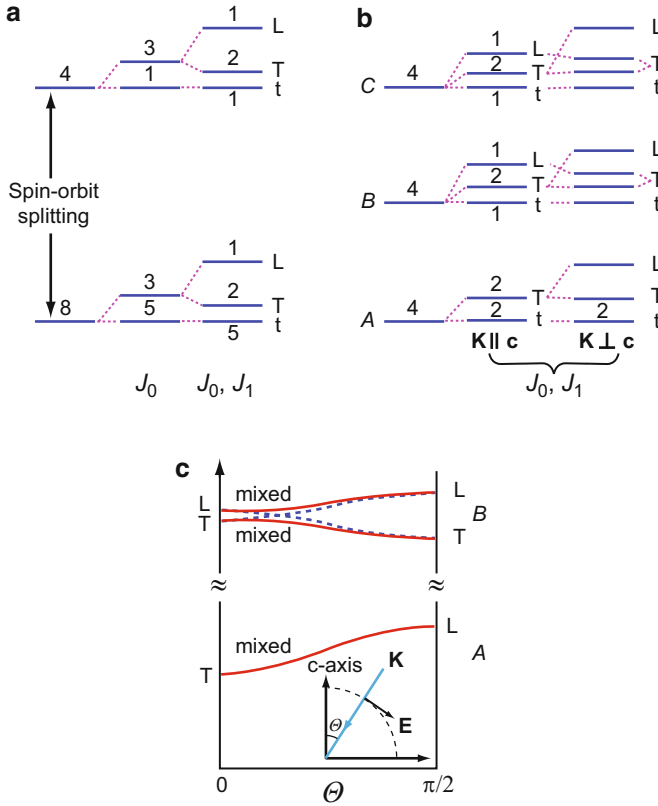


Fig. 10 Splitting of exciton levels for (a) cubic and (b) uniaxial crystals from the spin-triplet states (t) into dipole-allowed spin singlets and to the longitudinal (L) and transverse (T) dipole-allowed states due to exchange effects; numbers denote degeneracies. Levels in (b) are given for exciton wavevectors \mathbf{K} parallel and perpendicular to the crystal \mathbf{c} axis. (c) Mixed longitudinal and transverse modes of the A and B excitons as a function of the angle θ of \mathbf{K} with respect to \mathbf{c} (After Cho 1979)

Γ_5 exciton, which is twofold degenerate, and into the nondegenerate Γ_1 and Γ_2 exciton states. The $A(\Gamma_6)$ and $B(\Gamma_2)$ states are not affected by the exchange interaction. For details, see Denisov and Makarov (1973) and Flohrer et al. (1979) who model explicitly wurtzite CdS. The splitting for GaN is discussed by Rodina et al. (2001) and for ZnO by Lambrecht et al. (2002).

The *exciton-phonon interaction* depends strongly on the carrier-lattice coupling, which is weak for predominantly covalent semiconductors, intermediate for molecular crystals, and strong for ionic crystals (alkali halides). Excitons can interact with phonons in a number of different ways. One distinguishes exciton interaction (for reviews, see Vogl 1976 and Yu 1979) by:

- Nonpolar optical phonons via the deformation potential (a short-range interaction; Loudon 1963)

- Longitudinal optical phonons via the induced longitudinal electrical field (Fröhlich interaction; Fröhlich 1954)
- Acoustic phonons via the deformation potential for a large wavevector, since for $\mathbf{q} \cong 0$ the exciton experiences a nearly uniform strain resulting in a near-dc field, resulting in no interaction with the electrically neutral exciton (Kittel 1963)
- Piezoelectric acoustic phonons via the longitudinal component similar to the Fröhlich interaction (Mahan and Hopfield 1964)

Another interaction involves three-particle scattering among photons, phonons, and excitons, such as the relevant Brillouin and Raman scattering (see Yu 1979 and Reynolds and Collins 1981).

In solids with a strong coupling of electrons (and holes) with the lattice, the exciton–phonon interaction can become large enough to cause *self-trapping* of an exciton (Kabler 1964). This can be observed in predominantly ionic crystals with a large bandgap energy and occurs because of a large energy gain due to distortion of the lattice by the exciton. It results in a very large increase of the effective mass of the exciton, which is usually a Frenkel exciton. It is distinguished from a polaron by the short-range interaction of the exciton dipole, compared to the far reaching Coulomb interaction of the electron/polaron. The self-trapped exciton may be a significant contributor to photochemical reactions. It is best studied in alkali halides; for a review, see Toyozawa (1980) and Song and Williams (1993).

In anisotropic crystals with an external perturbation, we must consider the relative direction of the exciting optical polarization \mathbf{e} , the exciton wavevector \mathbf{K} , and the crystallographic axis \mathbf{c} . One distinguishes σ and π modes when \mathbf{e} is \perp or \parallel to the plane of incident light, respectively (*transverse and longitudinal excitons*). When the incident angle $\theta \neq 90^\circ$, mixed modes appear (Fig. 10c). The resulting exciton lines in cubic and hexagonal systems for $\mathbf{k} \perp \mathbf{c}$ and $\mathbf{k} \parallel \mathbf{c}$ are given in Fig. 10a, b.

Many of the band degeneracies are lifted when the crystal is exposed to internal or external perturbation. Internally, this can be done by alloying (Kato et al. 1970) and, externally, by external fields such as mechanical stress and electrical or magnetic fields (reviewed by Cho 1979).

1.2.3 Indirect-Gap Excitons

Indirect-gap excitons are associated with optical transitions to a satellite minimum at $\mathbf{K} \neq 0$. The energy of an indirect exciton is

$$E_{g,\text{exc}}^{(\text{indir})} = E_g^{(\text{indir})} - E_{\text{exc},n} + \frac{\hbar^2}{2\mu} (\mathbf{K} - \mathbf{q}_0)^2, \quad (20)$$

with μ as the reduced mass between the valence bands and the satellite minima of the conduction band. In order to compensate for the electron momentum \mathbf{k}_0 at the satellite minimum, the transition requires an absorption or emission of a phonon of appropriate energy and momentum. The phonon momentum \mathbf{q}_0 is equal to \mathbf{k}_0 (see Fig. 11).

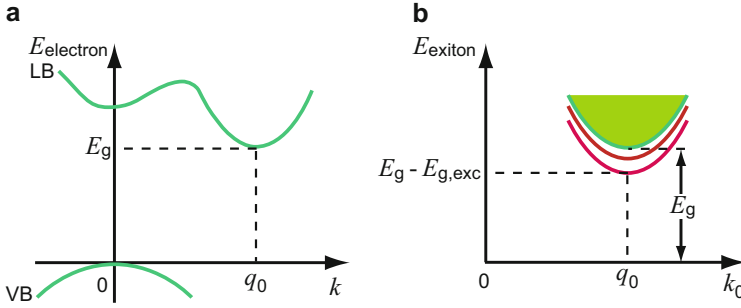


Fig. 11 Dispersion relation for indirect-bandgap excitons: (a) Typical band dispersion $E(k)$ of an indirect semiconductor. (b) Satellite minimum with ground and first excited state parabolas of indirect excitons

During the indirect excitation process, an electron and a hole are produced with a large difference in wavevectors. Such excitation can proceed to higher energies within the exciton dispersion using a slightly higher photon energy. The excess in the center-of-mass momentum is balanced by only a small change in phonon momentum. Therefore, we observe an onset for each branch of appropriate phonon processes for indirect-bandgap transitions, following selection rules, rather than a line spectrum observed for direct-bandgap material. Here, relaxing phonon processes are hardly observed since they have a much smaller probability.

One obtains for the absorption coefficient caused by these indirect transitions

$$\alpha_{o, cv, exc}^{(indir)} = \alpha_o^* \left[f_{BE} \sqrt{h\nu - E_g^{(indir)} + E_{g, exc, n} + \hbar\omega_q} + (f_{BE} + 1) \sqrt{h\nu - E_g^{(indir)} + E_{g, exc, n} - \hbar\omega_q} \right], \quad (21)$$

where α_o^* is a proportionality factor. This factor includes the absorption enhancement relating to the square of the exciton envelope function, and f_{BE} is the Bose–Einstein distribution function for the phonons. The two terms describe transitions with absorption and emission of a phonon, respectively. The allowed spectrum consequently has two edges for the ground state of the exciton, plus or minus the appropriate phonon energy. It is shown in Fig. 12b for the indirect gap of Ge. Excited exciton states disappear because of the strong $(1/n^3)$ dependence of the oscillator strength. The branch caused by phonon absorption also disappears at lower temperatures as less phonons are available.

For indirect-bandgap semiconductors like Ge, also transitions at $\mathbf{K} = 0$, i.e., direct-gap exciton transitions, can be observed; they proceed into a higher band above the bandgap. As an example, the exciton line near the direct transition at the Γ point of Ge at 0.883 eV for 77 K is shown in Fig. 12a, c.

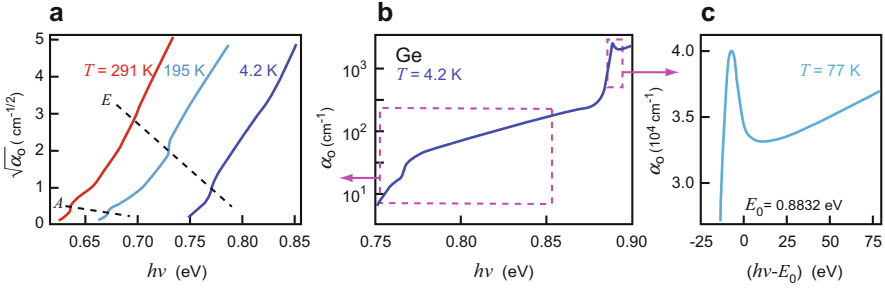


Fig. 12 (b) Weak indirect and strong direct excitonic transitions in Ge. (a) Detail of the indirect exciton transition preceding the band edge ($\Gamma_{8vb} \rightarrow \Gamma_{6cb}$) of Ge (After MacFarlane et al. 1957). *Dashed lines* indicate threshold for absorption (A) or emission (E) of a phonon. (c) Direct exciton at $k = 0$ and band-to-band transition from Γ_{8vb} into Γ_{7cb} of Ge at 77 K. Note different ordinate scalings

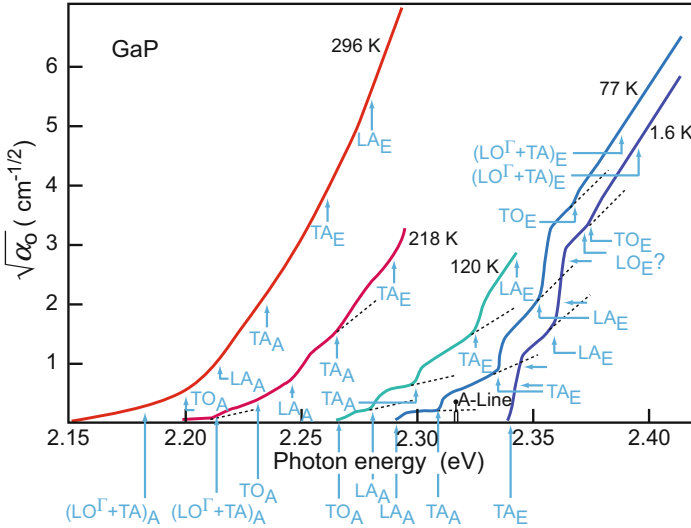


Fig. 13 Indirect exciton transition in GaP with threshold energies for indirect, phonon-assisted transitions at various temperatures. The additional absorption edges connected to different types of phonons or phonon pairs are identified accordingly (After Dean and Thomas 1966)

A more structured series of square-root shaped steps at the indirect excitonic transition is shown for GaP in Fig. 13. Here, different types of involved phonons are observed more pronounced. The corresponding energies of the absorbed or emitted phonons are 12.8, 31.3, and 46.5 meV for TA, LA, and LO phonons in GaP, respectively.

1.3 Exciton–Polaritons

In some of the previous sections, the interaction of light with electrons was described by near band-to-band transitions close to $\mathbf{K} = 0$, creating direct-bandgap excitons. This interaction requires a more precise analysis of the dispersion relation. The exciton and photon dispersion curves are similar to those for phonons and photons (Fig. 14). Both show the typical splitting due to the von Neumann noncrossing principle. In this range, the distinction between a photon and the exciton can no longer be made. The interacting particle is a polariton or, more specifically, an *exciton–polariton*.

Entering the resonance frequency for excitons into the polariton dispersion equation (► Eq. 68 of chapter “Photon–Phonon Interaction”) and including spatial dispersion ($\hbar^2 K^2 \omega_t^2 / \mu^2$), we obtain the *exciton–polariton equation*

$$v^4 - v^2 \left(v_l^2 + \frac{c^2 k^2}{\epsilon^*} \right) + \frac{c^2 K^2}{\epsilon^*} v_t^2 = 0 \quad (22)$$

with a kinetic energy term

$$h\nu_{(l,t)} = h\nu_{\text{exc}(l,t)} + \frac{\hbar^2 K^2}{2(m_n + m_p)}. \quad (23)$$

The ability of the exciton to move through the lattice represents propagating modes of excitation within the semiconductor. They are identified by the term $\propto K^2$ and have a group velocity ($\propto \partial E / \partial K$) on the order of 10^7 cm/s. Consequently, the dielectric constant is wavevector dependent and can be written as

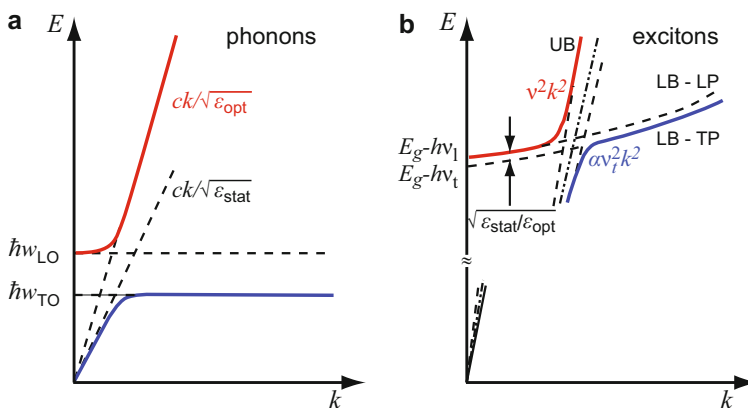
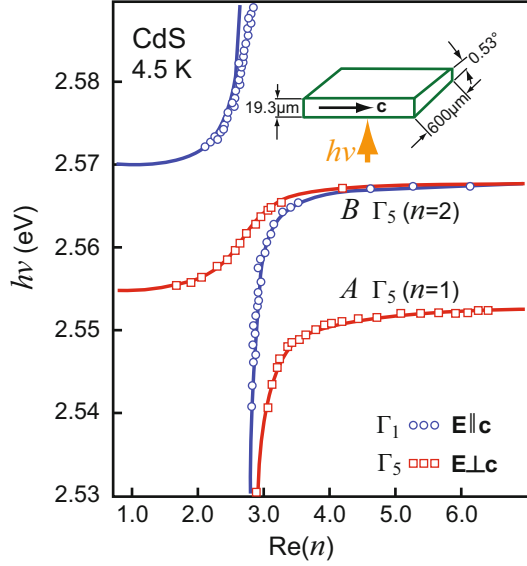


Fig. 14 Comparison between (a) a phonon–polariton and (b) an exciton–polariton (schematic and not to scale) with upper (UB)- and lower-branch (LB) longitudinal (LP) and transverse polaritons (TP)

Fig. 15 Energy of *A* and *B* exciton–polaritons as a function of the real part of the index of refraction for $\mathbf{E} \parallel$ and \perp to \mathbf{c} in a wedge-shaped CdS crystal compared to theoretical curves (After Broser et al. 1981)



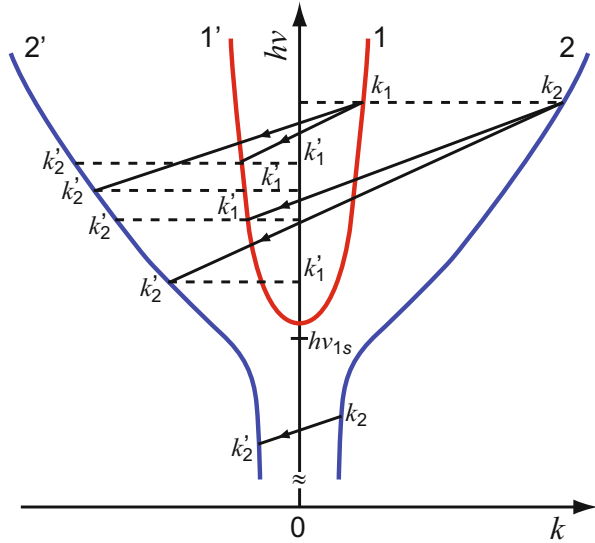
$$\epsilon^* = \epsilon_{\text{opt}} \left(1 + \frac{v_l^2 - v_t^2}{v_t^2 - v^2 + \beta K^2 - i\gamma v} \right), \text{ where } \beta = \frac{h v_t}{m_n + m_p}. \quad (24)$$

There is now an additional spatial dispersion term βK^2 in the denominator in contrast to an otherwise similar equation for the phonon–polaritons, which does not have spatial dispersion.

The polariton dispersion-equation has several branches. These branches depend on crystal anisotropy and the relative orientation of the polarization of light, exciton \mathbf{K} vector, and crystallographic axes. As many as four lower and two upper branches are predicted and observed by single- and two-photon excitation processes. An example is shown for CdS in Fig. 15, with upper and lower branches for longitudinal and transverse excitons pointed out; the given abscissa values are related to the wavevector by $\text{Re}(k) = (\omega/c)\text{Re}(\tilde{n})$. See also Girlanda et al. (1994); for a review, see Hönerlage et al. (1985).

If the impinging light has an energy below, but close to, a free exciton line in direct-bandgap semiconductors, a longitudinal acoustic phonon can supply the missing energy, and resonant Brillouin scattering with exciton–polaritons occurs. When the energy supplied by the photon lies below the $1S$ exciton, one observes a single backward scattered Stokes line at $h\nu_{1S}$ (Fig. 16) with a transition $k_2 \rightarrow k'_2$. When the frequency of the photon lies above $h\nu_{1S}$, four Stokes-shifted lines are expected, for which energy and momentum conservation is fulfilled. The same number of *blue*-shifted anti-Stokes lines is additionally observed (not shown in the figure for clarity). The exciton–polariton state is created with phonons near the center of the Brillouin zone, which interact strongly with optical radiation.

Fig. 16 Dispersion curves of free exciton–polaritons with inner (1, 1′) and outer branches (2, 2′), indicating the Stokes processes of Brillouin scattering between different branches



In contrast to the phonon–polariton scattering discussed in ► Sect. 3.1 of chapter “Photon–Phonon Interaction”, the lower branch of the exciton–polariton is not flat but parabolic in its upper part, since the exciton is mobile and can acquire kinetic energy which causes an $E \propto k^2$ behavior. In addition, there are several lower branches according to the different excited states of the exciton; for a review, see Yu (1979). A measured spectrum⁸, showing several of these branches from the ground and excited states of the exciton, is shown in Fig. 17. Some of these relate to interaction with LA phonons, others with TA phonons, as indicated in the figure.

Additional information about the exciton–polariton dispersion relation is obtained from *hyper-Raman scattering*. More intense optical excitation is required to induce a two-photon excitation of a virtual biexciton⁹ (see Fig. 18). Hyper-Raman scattering, when using two photons of frequencies ν_1 and ν_2 , each having an energy slightly below the bandgap energy and propagating with wavevectors \mathbf{k}_1 and \mathbf{k}_2 inside the semiconductor, creates a new intermediate state with

$$\mathbf{k}_1 + \mathbf{k}_2 = \mathbf{K} \text{ and } h\nu_1 + h\nu_2 = E(\mathbf{K}). \quad (25)$$

If the energy $h\nu_1 + h\nu_2$ is close to the resonant state (the biexciton), one observes a strongly enhanced transition (see Fröhlich 1981). The virtual biexciton decays into two quasiparticles, one of which is observed, while the other remains in the crystal to conserve energy and momentum. There are three possibilities:

⁸The analysis of the measured reflection spectrum as a function of the wavelength and incident angle is rather involved. A relatively simple method for measuring the central part of the exciton–polariton spectrum in transmission through a prismatic crystal was used by Broser et al. (1981) (see Fig. 13).

⁹A state close to an actual biexciton state (Sect. 1.4) which immediately decays into other states.

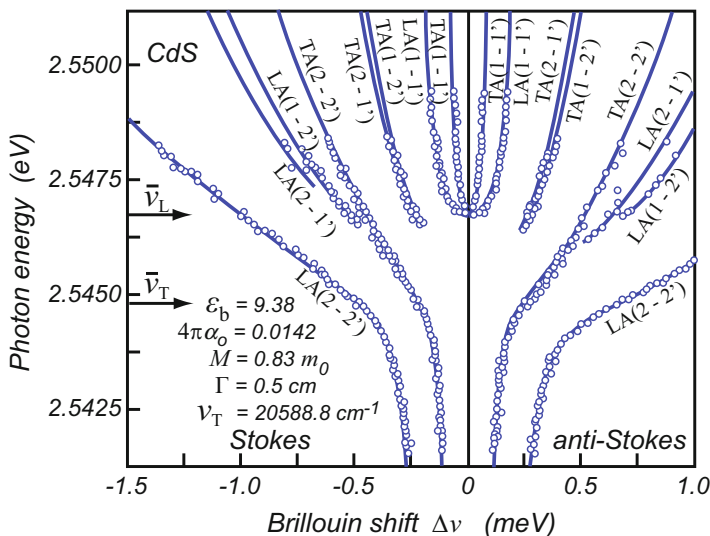


Fig. 17 Brillouin shift of the scattered laser light in CdS as a function of the laser energy. Theoretical transitions refer to the indexing shown in Fig. 16. Parameters: dielectric constant $\epsilon_b = 9.38$, oscillator strength $4\pi\alpha_0 = 0.0142$, excitonic mass $0.83 m_0$, phenomenological damping constant $\gamma = 0.5 \text{ cm}$, transverse exciton energy 2.5448 eV , and longitudinal exciton energy 2.5466 eV . The numerals 1 and 2 refer to inner and outer branch polaritons (After Wicksted et al. 1984)

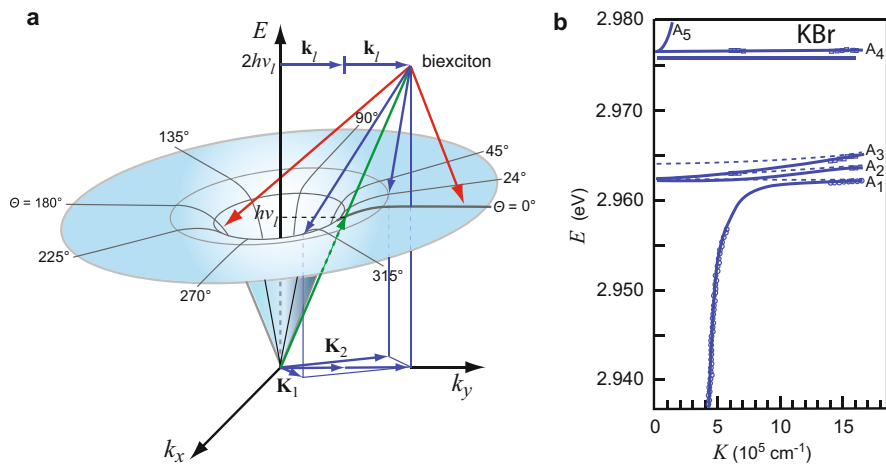


Fig. 18 (a) Hyper-Raman scattering illustrated by one lower polariton branch drawn in two dimensions (k_x, k_y). Exciting laser photon, $h\nu_l(k_i)$; virtual biexciton, $2h\nu_l(2k_i)$; indicated recombination, backscattering (red arrows) one polariton-like and one exciton-like state, arrow at 180° paired to arrow at 0° for leftover polariton; forward scattered pair, blue arrows as alternatives. (b) Dispersion curves of five branches of polaritons in CuBr for $\mathbf{e} \parallel [001]$ and $\mathbf{K} \parallel [110]$ (After Hönerlage et al. 1985)

$h\nu_1 + h\nu_2 = E_{\text{LP}}(\mathbf{K}_{\text{LP}}) + E_{\text{LP}}(\mathbf{K}_{\text{LP}})$ (two lower-branch polaritons)

$h\nu_1 + h\nu_2 = E_{\text{LP}}(\mathbf{K}_{\text{LP}}) + E_{\text{UP}}(\mathbf{K}_{\text{UP}})$ (one lower, one upper polariton)

$h\nu_1 + h\nu_2 = E_{\text{LP}}(\mathbf{K}_{\text{LP}}) + E_{\text{L,exc}}(\mathbf{K}_{\text{L,exc}})$ (one lower polariton, one longitudinal exciton)

For all of these alternatives, the condition

$$\mathbf{k}_1 + \mathbf{k}_2 = \mathbf{K}_i + \mathbf{K}_j \quad (26)$$

is fulfilled.

Figure 18a depicts the creation of a biexciton from two photons (two green arrows up) with energies $h\nu_1 = h\nu_2 = h\nu_l$ and wavevector $\mathbf{k}_1 = \mathbf{k}_2 = \mathbf{k}_l$ along the k_y axis; both photons are provided by the same laser with energy $h\nu_l$, and the biexciton has $2h\nu_l$ energy and $2\mathbf{k}_l$ wavevector. This biexciton decays into two lower polaritons (pair of red arrows down) which are offset by an angle to fulfill momentum conservation and land at different points ($h\nu$) on the polariton surface; one of these polaritons is observed, and θ is the scattering angle between incident photon and observed polariton. The point of landing depends on the energy of the initiating photon pair and the angle of observation of the emitted (scattered) photon [backscattering, small θ ($<30^\circ$), solid red arrows; forward scattering (observation through the sample), large θ , dashed arrows]. This makes hyper-Raman scattering a three-photon process; it is determined by the third-order term in the susceptibility. The entire polariton spectrum is obtained by changing the energy of the exciting light (the resulting virtual biexciton), the angle and energy of the emitted photon, and calculating energy and momentum of the leftover polariton. Several polariton branches have consequently been observed (Fig. 18b).

Hyper-Raman scattering follows selection rules other than those for normal Raman scattering or IR absorption. It thereby yields additional information about the lattice vibrational spectrum, e.g., about dipole modes in centrosymmetrical lattices which are forbidden in normal Raman scattering. It also permits excitation deep inside a crystal. For reviews, see Denisov et al. (1987) and Hönerlage et al. (1985); see also García-Cristóbal et al. (1998).

Besides the bulk polaritons discussed so far, there are also *surface-polariton modes*; they progress in a thin layer near the semiconductor surface and can be used to reveal properties of the crystal near the surface. Grazing incident light or reflection measurement is used for their detection (Hopfield and Thomas 1963); for Raman measurements, see Davydov et al. (1997). The region near the surface cannot be penetrated by bulk-excitons to a thickness of either the space-charge region at the surface or the bulk-exciton diameter, whichever is larger (Altarelli et al. 1979). These surface exciton-polaritons are reviewed by Fischer and Lagois (1979).

1.4 Trions and Biexcitons in Bulk Crystals

Free Trions An exciton can be weakly bound to an electron or another exciton to form a trion or biexciton, respectively (Lampert 1958; Moskalenko 1958; a proceeding on trions is found in Phys. Stat. Sol. B 227 (2), 2001). The trion is composed of either two electrons and a hole (this one is similar to an H^- ion) or two holes and an electron. Therefore, it is negatively or positively charged. Predicted by Gerlach (1974) and observed first by Thomas and Rice (1977), their binding energy in Ge is on the order of 0.2 meV; this trion has an effective mass of about 20% more than the sum of the free electron and hole masses, a radius about 50% larger than that of an exciton, and an ionization energy about 10% of the ionization energy of excitons.

Reports on *free* trions in semiconductors are scarce. Calculations yield states which are stable against dissociation into an exciton and a free carrier in both three-dimensional (3D) and lower-dimensional semiconductors. The binding energy (with respect to the exciton energy) depends on the ratio of electron and hole effective masses and is generally small for bulk semiconductors, typically one tenth for 3D trions compared to 2D quantum-well trions (Fig. 19); often experimental assignments are not unequivocal.

Characteristic features distinguish trions from excitons. Their formation is influenced by the position of the Fermi energy, as explicitly demonstrated for 2D trions (Sect. 2.2). In optical transitions, the initial electron or hole momentum is transferred to the final trion state, which leads to low-energy tails at the trion and exciton lines; in addition, exciton–electron scattering gives rise to a high-energy tail (trion continuum) at the exciton transition (Esser et al. 2001). In a magnetic field, trions show circularly polarized transitions for singlet and triplet states. Since trions have a significantly increased binding energy in low-dimensional semiconductors, they are well studied there and discussed in more detail in Sect. 2.

Fig. 19 Calculated binding energies of 3D and 2D negative (X^-) and positive trions (X^+) as a function of the electron and hole effective mass ratio (After Stébé and Ainane 1989). Energies are given with respect to the binding energy of a donor in a 3D crystal (The generally used symbol for trions is X^+ ; in initial work also the symbol X_2^+ was used, in analogy to a positively charged H_2^+ molecule)

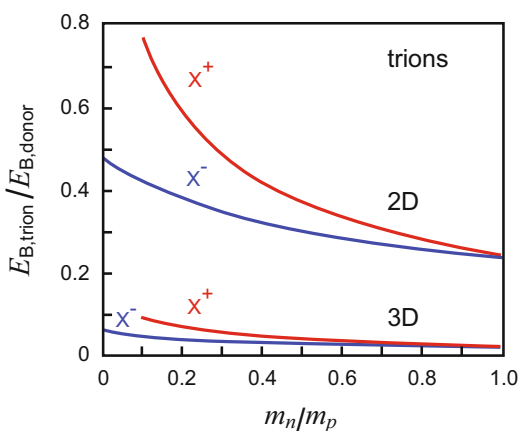
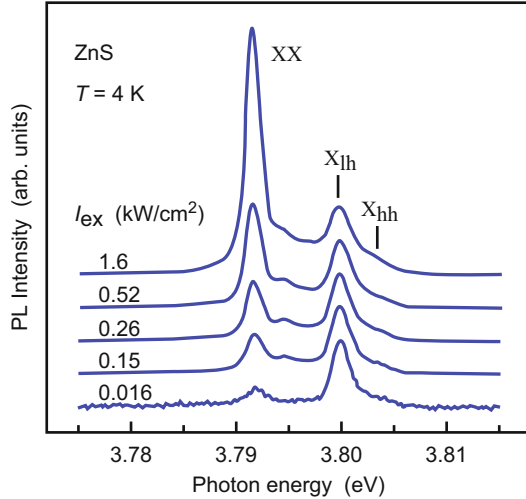


Fig. 20 Photoluminescence spectra of biexcitons (XX) and light- (X_{lh}) and heavy-hole exciton (X_{hh}) in a 6 μm -thick tensely strained ZnS layer on GaAs substrate. Spectra are normalized with respect to the peak intensity of the X_{lh} line (After Yamada et al. 2000)



Free Biexcitons Biexcitons are exciton molecules X_2 similar to a hydrogen molecule (when $m_p \gg m_n$) or a positronium molecule (when $m_p \cong m_n$). Biexcitons form a stable bound state of two excitons for all ratios of electron to hole effective masses and in all dimensions from 3D to 0D. The binding energy of a biexciton is higher than that of a trion and is typically of the order of 10–20% of that for an exciton. For isotropic bands, it decreases monotonically with increasing ratio of m_n/m_p from $E_B(X_2)/R_\infty^{eff}(X) \cong 0.3$ for $m_n/m_p \rightarrow 0$ to 0.03 for $m_n/m_p = 1$ (Akimoto and Hanamura 1972; Brinkman et al. 1973). This is similar to the decrease in relative binding energy from a hydrogen molecule $E_B(H_2)/R_\infty(H) = 4.7/13.6 = 0.35$ to the relative binding energy of a positronium (Ps) molecule $E_B(Ps_2)/E_B(Ps) = 0.13/6.8 = 0.02$. Such biexcitons have been observed in Si (Hanamura and Haug 1977; Thewalt and Rostworowski 1978) and can be observed readily in II–VI semiconductors (Zn and Cd chalcogens) or CuCl and CuBr (see Haken and Nikitine 1975 and Ueta and Nishina 1976). Biexciton and exciton spectra of a bulk-like thick ZnS layer are given in Fig. 20. Tensile strain splits the valence band of the zincblende ZnS into the heavy- and light-hole bands, each producing an exciton emission. The exciton emission increases approximately linearly with excitation intensity I_{ex} , while the biexciton emission increases roughly quadratically¹⁰ ($I_{X_{lh}} \propto I_{ex}^{1.1}$, $I_{XX} \propto I_{ex}^{1.9}$): the probability to form a biexciton molecule XX is proportional to the density of each of the two participating excitons X; the dominating line in Fig. 20 is the light-hole biexciton X_{lh} .

A high density of excitons hence favors the formation of biexcitons. However, the low binding energy requires low temperatures which, in turn, favors further

¹⁰Deviations from a pure quadratic dependence are due to the short radiative lifetime for the involved species in direct-bandgap semiconductors, preventing a thermal equilibrium of the population.

condensation into an electron–hole liquid (► Sect. 3.2 of chapter “Equilibrium Statistics of Carriers”). This condensation can be suppressed by applying a uniaxial stress (Gourley and Wolfe 1978) or biaxial strain as in epitaxial layers (Fig. 20); larger biexciton signals are then observed. Further discussion of excitonic molecules is provided by Kulakovskii et al. (1985).

The line shape of biexcitons, observed by luminescence or scattering experiments, is typically asymmetric (similar to that of trions) because of the recoil energy when they recombine: the line has a larger low-energy tail. During this process, there is always a remaining partner that can take up part of the energy as kinetic energy. For a review, see Hanamura (1976) and Hönerlage et al. (1985). At higher densities, excitons or excitonic molecules can no longer exist, but form an electron–hole plasma, as described in ► Sect. 3.2 of chapter “Equilibrium Statistics of Carriers”.

2 Excitons in Low-Dimensional Semiconductors

In low-dimensional semiconductors, the density of states is modified (► Sect. 3.2 and ► Fig. 37 of chapter “Bands and Bandgaps in Solids”), yielding an increase at the band-edge energy for gradually decreased dimensionality. In addition, the dielectric constant and effective mass are anisotropic and result in ellipsoidal excitonic eigenfunctions. The exciton binding-energy is increased by confining barriers, affecting energies of the Rydberg series, the Bohr radius, and the oscillator strength. We first focus on two-dimensional excitons.

2.1 Excitons in Quantum Wells

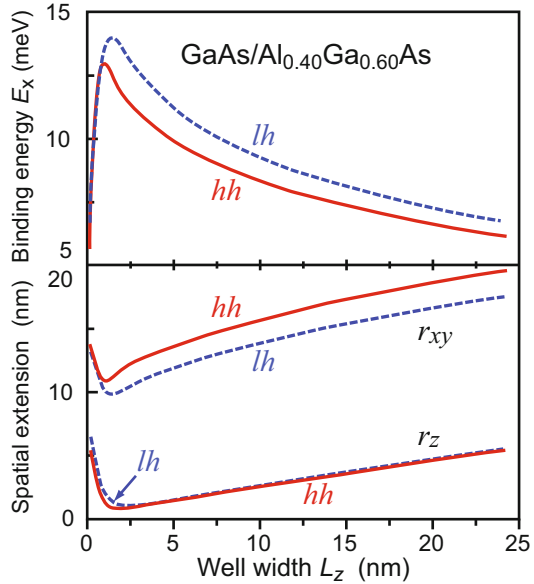
Carriers in a quantum well are free to move in two spatial directions (x, y), while confining barriers lead to quantized states in the third dimension (z) (see ► Sect. 3.1.1 of chapter “Bands and Bandgaps in Solids”). The confinement applies also for excitons, and the two-dimensional exciton energy gets

$$E_{g, \text{exc}, 2\text{D}} = E_g + E_z - R_\infty \frac{\mu}{m_0} \frac{1}{\epsilon_{\text{stat}}^2} \frac{1}{(n - \frac{1}{2})^2} + \frac{\hbar^2 (K_x^2 + K_y^2)}{2(m_n + m_p)} \text{ with} \quad (27)$$

$$n = 1, 2, \dots$$

Here, E_z is the energy of the quantization in z direction given by the quantum number $n_{\text{QW}} = 1$ in ► Eq. 54 of chapter “Bands and Bandgaps in Solids” for infinite barriers and shown in ► Fig. 31 of chapter “Bands and Bandgaps in Solids” for finite barriers. The third term is the effective Rydberg energy R_∞^{eff} (or binding energy $E_{\text{exc}, n=1}$; see Eq. 10); if the exciton wavefunction does not penetrate significantly into the barriers, the material parameters of R_∞^{eff} remain unchanged; consequently, the binding energy of the two-dimensional $1S$ exciton is increased by a factor of

Fig. 21 Calculated binding energy and spatial extension of heavy- (*hh*) and light-hole excitons (*lh*) in a GaAs/ $\text{Al}_{0.4}\text{Ga}_{0.6}\text{As}$ quantum well (After Grundmann and Bimberg 1988)



4 compared to the 3D 1S exciton (Shinada and Sugano 1966). In real quantum wells with finite barriers, the factor is smaller and depends on the well width (see Fig. 21). The confinement results in elliptical orbits with a highly compressed coordinate in the direction normal to the quantum-well plane. Here, the orbiting electron and hole approach each other closely, which causes the increase in their binding energy. Initial work on quantum wells was done by Dingle et al. (1974). For a review, see Ploog and Döhler (1983) and Miller and Kleinman (1985).

Since the binding energy depends on the well width, variations of this width by a roughness of the interfaces between well and barriers (also on a scale of atomic monolayers) also affect the binding energy. This applies not only to excitons but also to charged excitons (trions) and higher exciton complexes (Filinov et al. 2005). The binding energy depends also on the effective mass (see Eq. 27); since heavy and light holes have different effective masses, their splitting in exciton spectra can be used to measure the strain in quantum wells (Kudlek et al. 1992).

The increased binding energy and decreased spatial extension in two dimensions are accompanied by an increased oscillator strength f , originating from a larger overlap of the electron and hole wavefunctions. In three dimensions, $f(n) \propto n^{-3}$; in two dimensions n is replaced by $n - \frac{1}{2}$, yielding a substantial increase in transition probability. Exciton absorption in quantum wells causes the near-band edge features shown in ► Fig. 15 of chapter “Band-to-Band Transitions”. These Wannier–Mott excitons are observed in bulk material only at low temperatures, but remain visible to much higher temperatures in quantum wells. The substantially increased lifetime of excitons at higher temperatures is due to the increased exciton binding energy, which is caused by the two-dimensional confinement.

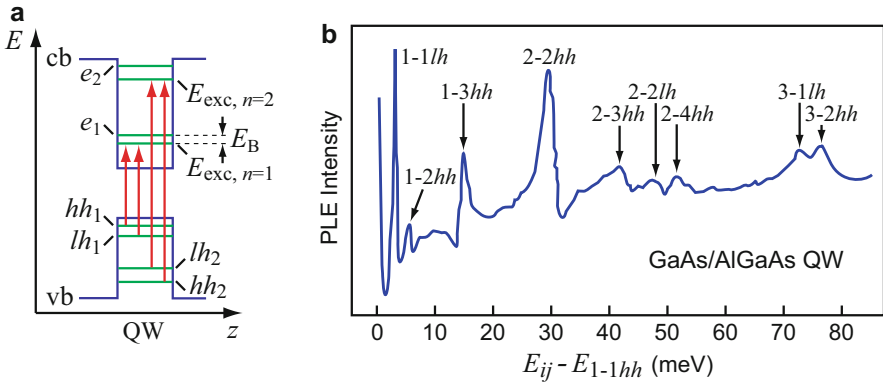


Fig. 22 (a) Exciton states for light (lh) and heavy holes (hh) with $1S$ exciton binding energy E_B indicated. Red arrows mark the strongest transitions. (b) Photoluminescence excitation (PLE) spectrum of hh valence- or lh valence-band excitons in a $L = 22$ nm-wide GaAs quantum well with AlGaAs barriers, measured at $T = 5$ K (After Koteles et al. 1987). The first and second indices identify the quantum level in the well of the conduction band and valence band, respectively; energies are given with respect to the e_1 - hh_1 exciton emission

In the energy diagram (Fig. 22a), the exciton energies are shown as lines below the electron levels e_i . The bonding energy of the $1S$ exciton is indicated as $E_B = e_1 - E_{exc, n=1}$. The exciton energy, however, lies above the gap energy of the well material (labeled by QW in Fig. 22a). We distinguish light- (lh) and heavy-hole (hh) excitons and excitons relating to the first or higher electron level. An example is given in Fig. 22b for a single GaAs/AlGaAs quantum well: excitons are shown combining up to the third conduction-band level with up to the fourth valence-band level.

The linewidth of the exciton absorption is given by its relaxation time (discussed in ► Sect. 2.2 of chapter “Dynamic Processes”). Additional broadening is caused by disorder in the alloy of the quantum well or the barriers and, particularly when severely confined, also by the quality of the well interfaces. Roughness in these interfaces causes broadening by well-width fluctuation (Bajaj and Reynolds 1987). At very low temperatures, well-size fluctuations are resolved as different spikes separated by < 1 meV, as shown by Yu et al. (1987).

Electric and uniaxial stress fields cause characteristic changes in the exciton spectrum of quantum wells. The electric field perpendicular to the layers causes a Stark shift toward longer wavelength. New peaks become visible, caused by transitions which were forbidden without perturbation, e.g., such from the m th level of the valence band to the n th level of the conduction band with $m \neq n$ (also seen for the strained QW in Fig. 22b). Such transitions become permitted because of a field-induced deformation of electron and hole eigenfunctions which now overlap. It is shown in Fig. 23a for 1-2 hh and 1-3 hh excitons which are not observed in these samples at zero bias. The changes in peak position with the electric field illustrate the anticrossing of two levels, demonstrating the von Neumann noncrossing rule when the states interact with each other (see Fig. 23b, c).

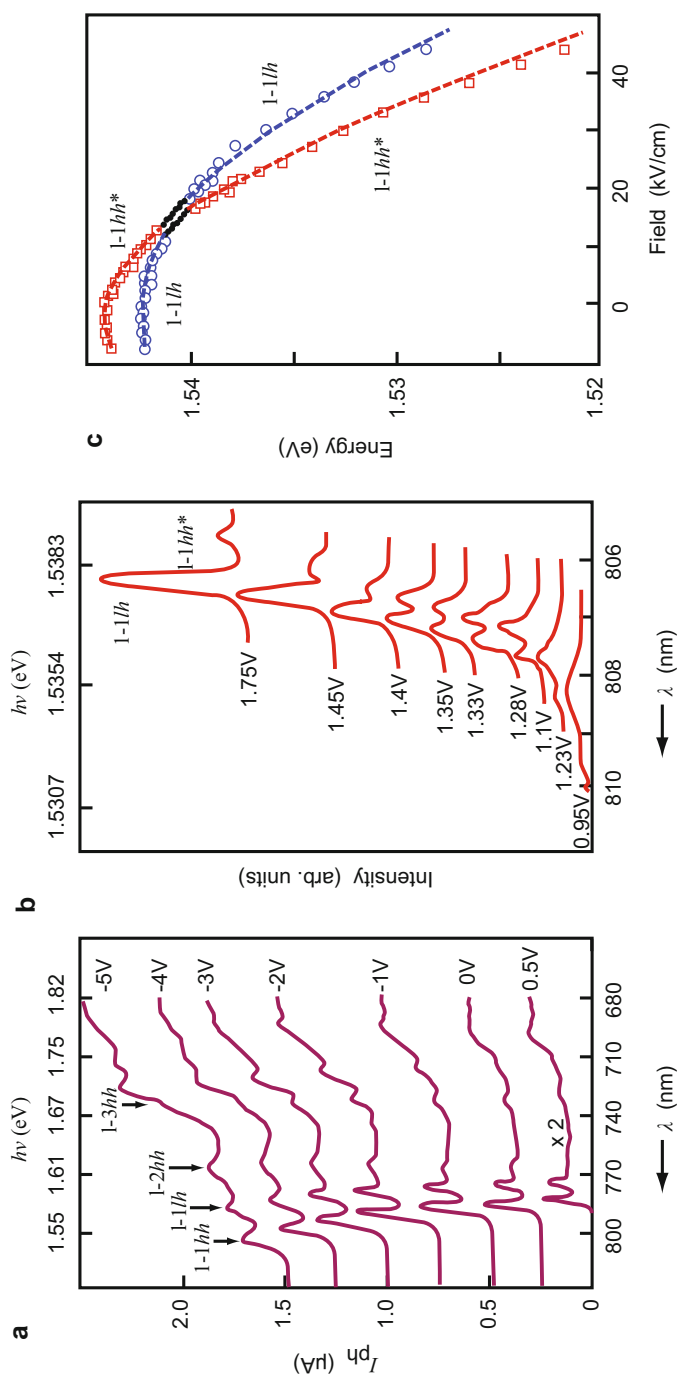


Fig. 23 Shift of exciton peaks with external electric field in GaAs/Al_{0.3}Ga_{0.7}As quantum wells. (a) Well width 8 nm, $T = 10$ K, applied voltage across 210 nm. (b, c) Anticrossing of the 2S state observed in the $1-1lh$ transition with the 1S state observed in the $1-1hh$ transition for 16 nm well width at 4.3 K. Data in the anticrossing region are shown as *solid circles*; the *dashed curves* are calculated Stark shifts neglecting exciton coupling. Family parameter is the applied voltage (After Collins et al. 1987)

Similarly, shifts and anticrossing of levels are observed when uniaxial stress is applied, as shown by Koteles et al. (1987) for the transitions given in Fig. 22b. For earlier works, see Miller et al. (1985).

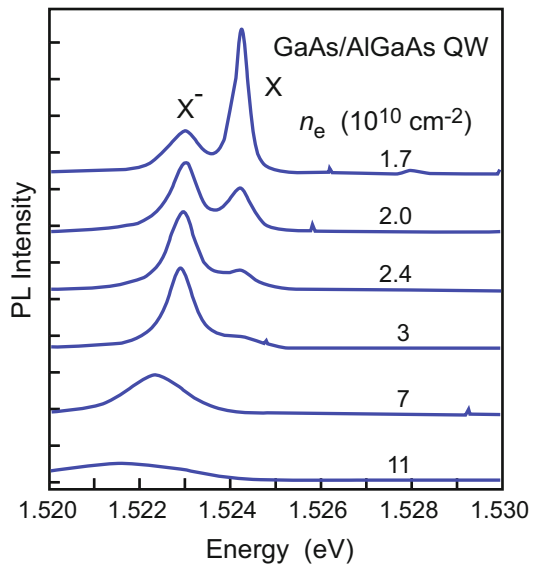
2.2 Biexcitons and Trions in Quantum Wells

Biexcitons and trions experience in low-dimensional structures a substantial increase of binding energy due to the confining potential similar to confined excitons.

Two-Dimensional Trions There are many reports on trions in quantum wells; for reviews, see Bar-Joseph (2005) and Shields et al. (1995a). A slight, often unintentional n -type or p -type doping provides excess carriers and increases the probability for $X^- = (e,e,h)$ or $X^+ = (e,h,h)$ formation, respectively, after creation of excitons. Using a modulation-doped quantum-well structure (similar to ► Fig. 11b of chapter “Photon–Free-Electron Interaction”), the two-dimensional remote electron density can be controlled, yielding an increased negative trion emission at higher electron density (see Fig. 24). Vice versa the reflectivity of the trion resonance was used to measure the carrier density (Astakhov et al. 2002a).

The separation between the X and X^- emissions in Fig. 24 is the binding energy of the trion, i.e., the energy of the second electron bound to the exciton. It varies with well width and reaches about 2 meV for X^- in 10 nm-wide GaAs QWs (Bar-Joseph 2005). Since trions can also be bound to donors which provide the remote electron density, the experimentally determined X^- binding energy may be overestimated; significantly smaller values (factor $1/2$) were evaluated from an extrapolation to large

Fig. 24 Negative trion photoluminescence in a modulation-doped GaAs/AlGaAs quantum well with an electron density controlled by a negative gate voltage. At high electron sheet-density, the heavy-hole exciton emission X disappears, and the trion emission X^- dominates (After Bar-Joseph 2005)



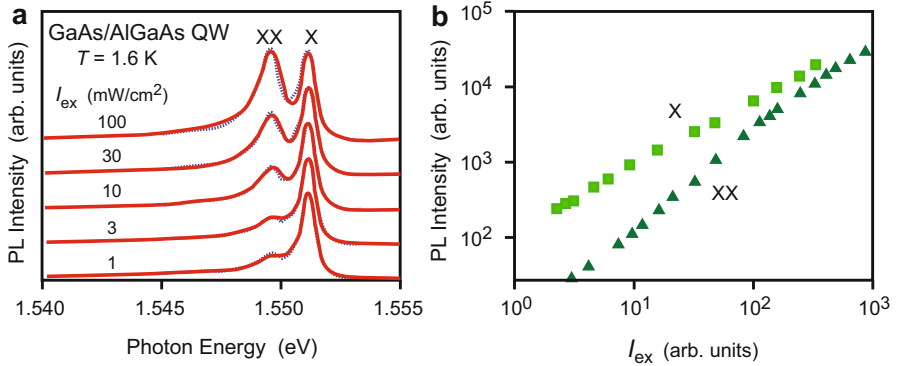


Fig. 25 (a) Biexciton emission (XX) in a GaAs/Al_{0.33}Ga_{0.67}As quantum well at different excitation levels. The spectra (blue) are normalized with respect to the exciton peak (X); continuous curves (red) are model calculations. (b) Dependence of exciton and biexciton luminescence intensity on excitation density (After Phillips et al. 1992)

donor distances for comparable GaAs QW samples (Solovyev and Kukushkin 2009). II–VI semiconductors have larger exciton and consequently also larger X^- binding energies. For ZnSe, up to 8.9 meV for thin QWs (2.9 nm) was determined for X^- and slightly smaller values for X^+ (Astakhov et al. 2002b).

The binding energy for the second hole in positively charged (X^+) trions should theoretically slightly exceed that of the second electron value for X^- by 17% in the 2D limit due to the larger hole effective mass (Stébé and Ainane 1989). Experimentally roughly similar values are observed due to the uncertainties noted above and the quite small difference (Shields et al. 1995b).

Two-Dimensional Biexcitons A biexciton binding energy of $\sim 22\%$ of the respective exciton binding energy was calculated for quantum wells (Singh et al. 1996), in agreement with experimental values (Birkedal et al. 1996). This implies a largely similar dependence of the binding energy on QW width for both biexcitons (XX) and excitons (X), a finding also observed in quantum dots (Zieliński et al. 2015). Values are typically slightly larger than for trions.

The superlinear increase of the biexciton emission-line with increase of excitation density I_{ex} is shown for a GaAs/AlGaAs quantum well in Fig. 25. Similar to the bulk case (Fig. 20), the measured dependence of biexciton to exciton intensity $I_{\text{XX}} \propto I_{\text{X}}^{1.6}$ has an exponent below 2 due to the short radiative lifetime; the displayed XX and X lines are from heavy-hole excitons.

2.3 Excitons in Quantum Wires and Quantum Dots

Starting from a two-dimensional quantum well, further reduction of dimensionality toward a one-dimensional quantum wire or a zero-dimensional quantum dot

requires some patterning to define an additional lateral confinement. The small dimensions needed to obtain quantum-size effects can usually not be accomplished by patterning a quantum-well structure using lithography techniques: the electronic properties of such structures are governed by interface defects. A variety of techniques was developed instead to realize 1D and 0D structures with high optical quality (see ▶ Sect. 2.2 of chapter “The Structure of Semiconductors”). Most of these techniques lead to complicate confinement potentials, and often an additional quantum well is coupled to the quantum wires or quantum dots.

2.3.1 Excitons in Quantum Wires

Work on epitaxial quantum wires (QWRs) was mostly performed using a V-shaped or T-shaped geometry (see ▶ Sect. 2.2.2 and ▶ Fig. 20 of chapter “The Structure of Semiconductors”). Structures based on GaAs are particularly well studied; the effective-mass approximation describes quantum effects quite good, and the fabrication technology is well developed. The lateral confinement of commonly used wire geometries is small, typically 30–40 meV, leading to small subband energy spacings of only 10 meV. For a review, see Akiyama (1998) and Wang and Voliotis (2006). Another approach for fabricating QWRs is whisker growth-forming nanowires (▶ Fig. 22 of chapter “The Structure of Semiconductors”) or colloidal synthesis of nanorods. In these structures, the confinement and dielectric contrast to the environment is larger than in epitaxial structures.

The exciton binding energy in a 1D quantum wire is expected to be stronger than in 2D or 3D. Analytical solutions of the Schrödinger equation for eigenenergies of states bound in a bare Coulomb potential for d dimensions ($d = 1, 2, 3, \dots$) yield in each dimension a Rydberg series (Ogawa and Takagahara 1991):

$$E_n^{(d)} = -R_\infty^{\text{eff}} \left(n + \frac{d-1}{2} \right)^{-2}, \quad n = 0, 1, 2, \dots \quad (28)$$

For 3D and 2D, we recognize the Rydberg series of hydrogen in Eq. 2 and 2D excitons in Eq. 27. For 1D a singularity occurs for the lowest state $n = 0$; the $1/r$ singularity of the Coulomb potential is removed upon integration in 2D and 3D, but it remains as a logarithmic singularity in 1D. This suggests the attractive force between electron and hole being stronger in 1D than in 2D or 3D. In a descriptive picture a particle may move *around* the origin of a Coulomb potential in 2D or 3D, while it moves *through* the origin in 1D. Experimentally, an enhancement of the exciton binding energy to 27 ± 3 meV (six to seven times larger than the bulk value) was observed in T-shaped quantum wires (Someya et al. 1996); binding energies exceeding 100 meV were found in semiconductor–insulator quantum wires (nanowires), where the effect is further enhanced by the strong dielectric contrast (Muljarov et al. 2000; Giblin et al. 2011).

Luminescence properties of one-dimensional excitons confined in a V-shaped quantum wire are shown in Fig. 26. The GaAs QWR is formed at the bottom of an AlGaAs V groove and has a crescent-like shape (▶ Fig. 21 of chapter “The Structure of Semiconductors”); at the groove sidewalls, additional quantum wells are formed

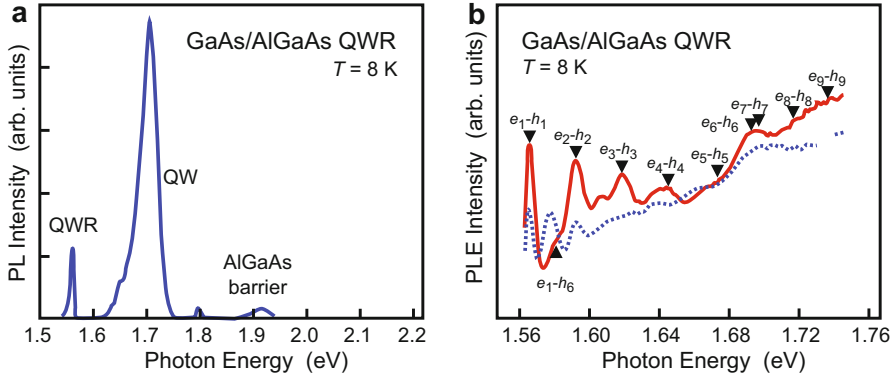


Fig. 26 (a) Photoluminescence (PL) of a 2.5 nm-thick V-shaped GaAs/Al_{0.3}Ga_{0.7}As quantum wire (QWR); the strong QW luminescence originates from sidewall quantum-wells. (b) PL excitation spectra polarized parallel (solid line) or perpendicular (dotted line) the [110]-oriented wire. Arrows mark calculated positions of excitonic e_n-h_m interband transitions (After Vouilloz et al. 1997)

during deposition of the upper AlGaAs barrier material, giving rise to the dominating luminescence in panel *a*. Placing the spectrometer on the QWR emission and varying the energy of the excitation photons yields the PLE spectrum shown in panel *b*. Labels mark exciton transitions, which similar to quantum wells are strong when quantum numbers of electrons and hole states are equal. An assignment of the transitions is not trivial due to the complicate geometry of the confinement potential; the transition energies indicated in Fig. 26b refer to model calculations, using a QWR shape extracted from electron micrographs. No distinction between heavy and light holes is made: the calculations reveal a strong mixing of the light- and heavy-hole character in the valence-band states (Vouilloz et al. 1998).

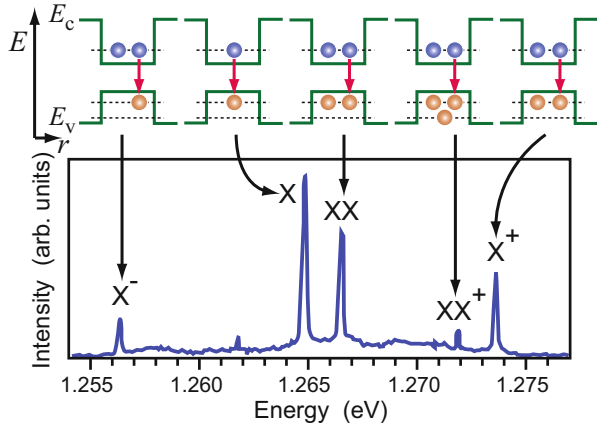
2.3.2 Excitons in Quantum Dots

The confinement in all three spatial directions leads to fully quantized electron and hole states of quantum-dot excitons without a kinetic contribution. Exciton transitions are consequently sharp like the discrete spectral lines of atoms.¹¹ The three-dimensional confinement may prevent dissociation of exciton complexes which are not stable in presence of a translational degree of freedom.

Excitonic emission from a single quantum dot is employed to create single photons on demand (Shields 2007); such single-photon sources are required for

¹¹Still a significant broadening of exciton transitions (of single quantum dots) well above the natural linewidth is observed due to the interaction of the quantum dot with its environment. The interaction with acoustic phonons (deformation potential coupling) and optical phonons (Fröhlich coupling) leads to broad transitions at increased temperature (Rudin et al. 1990); in addition, randomly fluctuating electrical fields of charged defects in the vicinity of the dots lead to a spectral jitter of the transitions on a very short time scale (spectral diffusion) even at low temperature (Türk et al. 2000).

Fig. 27 *Bottom:* Luminescence of a single InAs/GaAs quantum dot showing sharp recombination transitions of neutral and charged excitations and biexcitons (After Rodt et al. 2005). *Top:* Schematic band structure of carriers confined in the quantum dot with recombining electron (blue) and hole (red) indicated



quantum light generation applied, e.g., for intrinsically secure data transmission using quantum-key distribution (Scarani et al. 2009). The excitonic emission spectrum of a single quantum dot shown in Fig. 27 is dominated by the recombination of the neutral exciton labeled X ; in addition emissions from positively and negatively charged excitons (X^- , X^+) and those of neutral (XX) and positive biexcitons (XX^+) are observed. We note that the emission energy of several lines is *greater* than that of the exciton; this means that their binding energy with respect to the exciton energy is *negative*: they are in an antibinding state. The energy to keep the particles in a combined state is provided by the 3D confinement.

The binding energy of the exciton complexes depends on the size of the quantum dots. The binding energies of the biexciton (XX) and the positive trion (X^+) increase as the exciton energy decreases, i.e., for larger quantum dots (Fig. 28b); in this trend, the biexciton changes from antibinding to a binding state, as also indicated in Fig. 28a. The negative trion (X^-) is largely unaffected by the QD size and has always positive binding energy (i.e., the emission is shifted to the red). These features originate from the Coulomb interaction and correlation of the confined particles. The negative trion consists of two electrons and one hole confined in the QD; its binding energy is governed by the difference between the two Coulomb terms $C(e,h)$ and $C(e,e)$. The binding energy of the positive trion X^+ correspondingly depends on $C(e,h)$ and $C(h,h)$. Due to the larger effective mass of holes and the small size of the QDs, the wavefunction of the hole is stronger localized than that of the electron. Consequently $|C(e,e)| < |C(e,h)| < |C(h,h)|$ and the negative trion has a positive binding energy, while the positive trion has a negative binding energy. Calculations show that the *trend* is due to the number of bound hole states in the QD (Rodb et al. 2005); larger dots (smaller exciton energy) have more bound states and consequently more configuration interaction and increased binding energy.

The splitting of the exciton emission shown in Fig. 28a for different polarization directions is called fine-structure splitting. It appears in reversed order also in the biexciton emission, and for varied QD sizes, it has a trend comparable to that of the biexciton binding energy (Seguin et al. 2005). The mirrored appearance in the

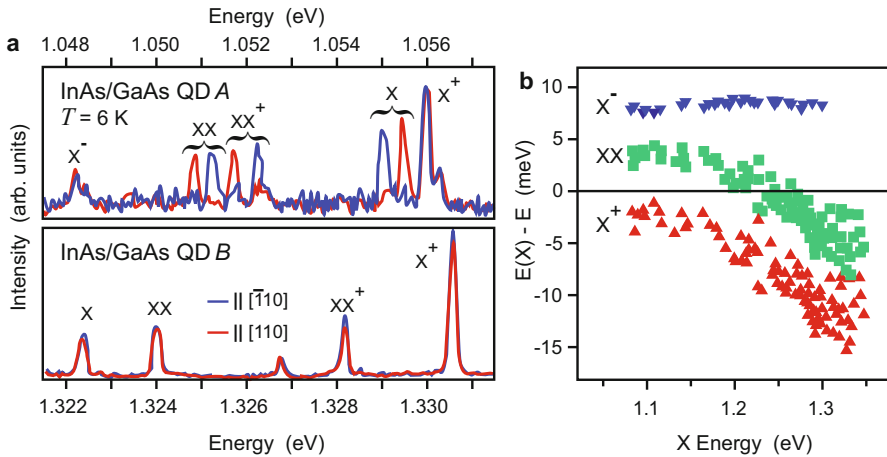


Fig. 28 (a) Exciton and biexciton luminescence of a large (*top*) and a small InAs/GaAs quantum dot (*bottom*) for linear polarization along the in-plane $\bar{1}10$ or 110 directions. (b) Energy differences between the recombination energies of confined exciton complexes (X^- , XX , X^+) and the neutral exciton (X) as a function of the exciton emission-energy (After Pohl 2008)

exciton and biexciton emission is due to the splitting of the exciton state, which is the final state of the radiative recombination of the biexciton XX to an exciton X (the biexciton state and the exciton ground state are unsplit). Studies of the fine-structure splitting received much advertece, since the radiative biexciton–exciton cascade can be employed to create pairs of entangled single photons for quantum optics and quantum-cryptography applications, if the splitting is smaller than the linewidth; for a review, see Shields (2007).

3 Summary

Excitons are quasiparticles combining an electron and a hole within their mutual Coulomb field; they resemble hydrogen atoms, except that the positively charged partner is not a heavy proton but a hole of about the same mass as an electron. Excitons show a hydrogen-like excitation spectrum; however, because of the perturbation from the lattice, other than S states are also observed in optical transitions, while in a free hydrogen atom, all optical transitions are equivalent to transitions between S states. One distinguishes large (Wannier–Mott) and small (Frenkel) excitons. Large excitons, with a typical diameter above three lattice constants, have a small ionization energy, typically on the order of 20 meV, while small excitons have ionization energies on the order of 1 eV. Wannier–Mott excitons are found in typical, mostly covalent semiconductors with large dielectric constant and small effective mass, while Frenkel excitons are found in ionic or organic molecule crystals. Many kinds of excitons are observed depending on the type of hole within the light, heavy, or spin–orbit split-off band and on the type of

electron: from a band at Γ (a direct exciton) or from a satellite valley (an indirect exciton). The interaction of an exciton with a charge carrier may form a charged exciton, a trion; similarly neutral or charged biexcitons can be formed. The binding energy of such free exciton molecules or higher associates is typically well below 20% of the exciton binding energy.

In low-dimensional semiconductors the binding energy and oscillator strength of all excitonic associates are significantly enhanced. Strongest transitions of confined excitons occur between electron and hole states of equal principal quantum numbers, similar to bulk excitons. In quantum dots, the three-dimensional confinement allows for forming stable antibinding exciton associates.

Excitons have a profound effect on the optical absorption spectrum by permitting absorption slightly below the corresponding band edge and by substantially increasing the absorption near the edge, but inside the intrinsic band-to-band range. Their analysis permits significant insight into the bonding type of the semiconductor, the dielectric function, and effective mass, all of which influence the spectrum. In low-dimensional semiconductors, they can be used as an optical probe of the perfection of the interlayer boundaries on an atomic scale and can also be used to analyze in detail the influence of a variety of field perturbations, e.g., internal strain. As such, they offer an important potential for analytical purposes.

References

- Akimoto O, Hanamura E (1972) Excitonic molecule. I. Calculation of the binding energy. *J Phys Soc Jpn* 33:1537
- Akiyama H (1998) One-dimensional excitons in GaAs quantum wires. *J Phys Condens Matter* 10:3095
- Altarelli M, Bachelet G, Del Sole R (1979) Theory of exciton effects in semiconductor surface spectroscopy. *J Vac Sci Technol* 16:1370
- Astakhov GV, Kochereshko VP, Yakovlev DR, Ossau W, Nürberger J, Faschinger W, Landwehr G, Wojtowicz T, Karczewski G, Kossut J (2002a) Optical method for the determination of carrier density in modulation-doped quantum wells. *Phys Rev B* 65:115310
- Astakhov GV, Yakovlev DR, Kochereshko VP, Ossau W, Faschinger W, Puls J, Henneberger F, Crooker SA, McCulloch Q, Wolverson D, Gippius NA, Waag A (2002b) Binding energy of charged excitons in ZnSe-based quantum wells. *Phys Rev B* 65:165335
- Bajaj KK, Reynolds DC (1987) An overview of optical characterization of semiconductor structures and alloys. *Proc SPIE* 0794:2
- Baldeschi A, Lipari NO (1973) Spherical model of shallow acceptor states in semiconductors. *Phys Rev B* 8:2697
- Bar-Joseph I (2005) Trions in GaAs quantum wells. *Semicond Sci Technol* 20:R29
- Bassani F, Pastori-Parravicini G (1975) *Electronic states and optical transitions in solids*. Pergamon Press, Oxford
- Beinikhes IL, Kogan ShM (1985) Influence of valence band degeneracy on the fundamental optical absorption in direct-gap semiconductors in the region of exciton effects. *Sov Phys JETP* 62:415
- Birkedal D, Singh J, Lyssenko VG, Erland J, Hvam JM (1996) Binding of quasi-two-dimensional biexcitons. *Phys Rev Lett* 76:672
- Brinkman WF, Rice TM, Bell B (1973) The excitonic molecule. *Phys Rev B* 8:1570

- Broser I, Broser R, Beckmann E, Birkicht E (1981) Thin prism refraction: a new direct method of polariton spectroscopy. *Solid State Commun* 39:1209
- Cavenett BC (1980) Optical detection of exciton resonances in semiconductors. *J Phys Soc Jpn* 49(Suppl A):611
- Cavenett BC (1984) Triplet exciton recombination in amorphous and crystalline semiconductors. *J Lumin* 31/32:369
- Cho K (1979) Internal structure of excitons. In: Cho K (ed) *Excitons*. Springer, Berlin, p 15
- Collins RT, Vina L, Wang WI, Mailhiet C, Smith DL (1987) Electronic properties of quantum wells in perturbing fields. *Proc SPIE* 0792:2
- Compaan A (1975) Surface damage effects on allowed and forbidden phonon Raman scattering in cuprous oxide. *Solid State Commun* 16:293
- Davies JJ, Cox RT, Nicholls JE (1984) Optically detected magnetic resonance of the triplet state of copper-center – donor pairs in CdS. *Phys Rev B* 30:4516
- Davydov VYu, Subashiev AV, Cheng TS, Foxon CT, Goncharuk IN, Smirnov AN, Zolotareva RV, Lundin WV (1997) Surface polariton Raman spectroscopy in cubic GaN epitaxial layers. *Mater Sci Forum* 264:1371
- Dean PJ, Thomas DG (1966) Intrinsic absorption-edge spectrum of gallium phosphide. *Phys Rev* 150:690
- Denisov MM, Makarov VP (1973) Longitudinal and transverse excitons in semiconductors. *Phys Status Solidi B* 56:9
- Denisov VN, Mavrin BN, Podobedov VB (1987) Hyper-Raman scattering by vibrational excitations in crystals, glasses and liquids. *Phys Rep* 151:1
- Dingle R, Wiegmann W, Henry CH (1974) Quantum states of confined carriers in very thin $\text{Al}_x\text{Ga}_{1-x}\text{As-GaAs-Al}_x\text{Ga}_{1-x}\text{As}$ heterostructures. *Phys Rev Lett* 33:827
- Elliott RJ (1961) Symmetry of excitons in Cu_2O . *Phys Rev* 124:340
- Esser A, Zimmermann R, Runge E (2001) Theory of trion spectra in semiconductor nanostructures. *Phys Status Solidi B* 227:317
- Filinov AV, Riva C, Peeters FM, Lozovik YuE, Bonitz M (2005) Influence of well-width fluctuations on the binding energy of excitons, charged excitons, and biexcitons in GaAs-based quantum wells. *Phys Rev B* 70:035323
- Fischer B, Lagois J (1979) Surface exciton polaritons. In: Cho K (ed) *Excitons*. Springer, Berlin, p 183
- Flohner J, Jahne E, Porsch M (1979) Energy levels of A and B excitons in wurtzite-type semiconductors with account of electron-hole exchange interaction effects. *Phys Status Solidi B* 91:467
- Frenkel JI (1931) On the transformation of light into heat in solids II. *Phys Rev* 37:1276
- Fröhlich H (1954) Electrons in lattice fields. *Adv Phys* 3:325
- Fröhlich D (1981) Aspects of nonlinear spectroscopy. In: Treusch J (ed) *Festkörperprobleme. Advances in solid state physics*, vol 21. Vieweg, Braunschweig, p 363
- García-Cristóbal A, Cantarero A, Trallero-Giner C, Cardona M (1998) Resonant hyper-Raman scattering in semiconductors. *Phys Rev B* 58:10443
- George GA, Morris GC (1970) The absorption, fluorescence and phosphorescence of single crystals of 1,2,4,5-tetrachlorobenzene and 1,4-dichlorobenzene at low temperatures. *Mol Cryst Liq Cryst* 11:61
- Gerlach B (1974) Bound states in electron-exciton collisions. *Phys Status Solidi B* 63:459
- Giblin J, Vietmeyer F, McDonald MP, Kuno M (2011) Single nanowire extinction spectroscopy. *Nano Lett* 11:3307
- Girlanda R, Savasta S, Quattropani A (1994) Theory of exciton-polaritons in semiconductors with nearly degenerate exciton levels. *Solid State Commun* 90:267
- Gislason HP, Monemar B, Dean PJ, Herbert DC, Depinna S, Cavenett BC, Killoran N (1982) Photoluminescence studies of the 1.911-eV Cu-related complex in GaP. *Phys Rev B* 26:827
- Gourley PL, Wolfe JP (1978) Spatial condensation of strain-confined excitons and excitonic molecules into an electron-hole liquid in silicon. *Phys Rev Lett* 40:526. And: Properties of the electron-hole liquid in Si: zero stress to the high-stress limit. *Phys Rev B* 24:5970 (1981)

- Grosmann M (1963) The effect of perturbations on the excitonic spectrum of cuprous oxide. In: Kuper CG, Whitfield GD (eds) *Polarons and excitons*. Oliver and Boyd, London, p 373
- Grundmann M, Bimberg D (1988) Anisotropy effects on excitonic properties in realistic quantum wells. *Phys Rev B* 38:13486
- Haken H (1963) Theory of excitons II. In: Kuper CG, Whitfield GD (eds) *Polarons and excitons*. Oliver and Boyd, Edinburgh, p 295
- Haken H (1976) *Quantum field theory of solids*. North Holland Publishing, Amsterdam
- Haken H, Nikitine S (eds) (1975) *Excitons at high densities*. Springer tracts in modern physics. Springer, New York
- Hanamura E (1976) Excitonic molecules. In: Seraphin BO (ed) *Optical properties of solids*. North Holland Publishing, Amsterdam, pp 81–142
- Hanamura E, Haug H (1977) Condensation effects of excitons. *Phys Rep* 33:209
- Hönerlage B, Lévy R, Grun JB, Klingshirn C, Bohnert K (1985) The dispersion of excitons, polaritons and biexcitons in direct-gap semiconductors. *Phys Rep* 124:161
- Hopfield JJ, Thomas DG (1963) Theoretical and experimental effects of spatial dispersion on the optical properties of crystals. *Phys Rev* 132:563
- Kabler MN (1964) Low-temperature recombination luminescence in alkali halide crystals. *Phys Rev* 136:A1296
- Kamtekar KT, Monkman AP, Bryce MR (2010) Recent advances in white organic light-emitting materials and devices (WOLEDs). *Adv Mater* 22:572
- Kato Y, Yu CI, Goto T (1970) The effect of exchange interaction on the exciton bands in CuCl-CuBr solid solutions. *J Phys Soc Jpn* 28:104
- Kazmierczuk T, Fröhlich D, Scheel S, Stolz H, Bayer M (2014) Giant Rydberg excitons in the copper oxide Cu₂O. *Nature* 514:343
- Kittel C (1963) *Quantum theory of solids*. Wiley, New York, p 131
- Kittel C (1966) *Introduction to solid state physics*. Wiley, New York
- Knox RS (1984) Introduction to exciton physics. In: DiBartolo B, Danko J (eds) *Collective excitations in solids*. Plenum Press, New York, p 183
- Koteles ES, Jagannath C, Lee J, Vassell MO (1987) Uniaxial stress as a probe of valence subband mixing in semiconductor quantum wells. *Proc SPIE* 0792:168
- Kudlek G, Presser N, Pohl UW, Gutowski J, Lilja J, Kuusisto E, Imai K, Pessa M, Hingerl K, Sitter A (1992) Exciton complexes in ZnSe layers: a tool for probing the strain distribution. *J Cryst Growth* 117:309
- Kulakovskii VD, Lysenko VG, Timofeev VB (1985) Excitonic molecules in semiconductors. *Sov Phys Usp* 28:735
- Lambrecht WRL, Rodina AV, Limpijumngong S, Segall B, Meyer BK (2002) Valence-band ordering and magneto-optic exciton fine structure in ZnO. *Phys Rev B* 65:075207
- Lampert MA (1958) Mobile and immobile effective-mass-particle complexes in nonmetallic solids. *Phys Rev Lett* 1:450
- Landau LD (1933) Electron motion in crystal lattices. *Phys Z Sowjetunion* 3:664
- Loudon R (1963) Theory of first-order Raman effect in crystals. *Proc R Soc Lond* A275:218
- MacFarlane GG, McLean TP, Quarrington JE, Roberts V (1957) Fine structure in the absorption-edge spectrum of Ge. *Phys Rev* 108:1377
- Mahan GD, Hopfield JJ (1964) Piezoelectric polaron effects in CdS. *Phys Rev Lett* 12:241
- McLean TP (1963) Excitons in germanium. In: Kuper CG, Whitfield GD (eds) *Polarons and excitons*. Oliver and Boyd, London, p 367
- Miller RC, Kleinman DA (1985) Excitons in GaAs quantum wells. *J Lumin* 30:520
- Miller DAB, Chemla DS, Damen TC, Gossard AC, Wiegmann W, Wood TH, Burrus CA (1985) Electric field dependence of optical absorption near the band gap of quantum-well structures. *Phys Rev B* 32:1043
- Moskalenko SA (1958) The theory of Mott exciton in alkali-halide crystals. *Zh Opt Spektrosk (USSR)* 5:147

- Mott NF (1938) Conduction in polar crystals. II. The conduction band and ultra-violet absorption of alkali-halide crystals. *Trans Faraday Soc* 34:500
- Muljarov EA, Zhukov EA, Dneprovskii VS, Masumoto Y (2000) Dielectrically enhanced excitons in semiconductor-insulator quantum wires: theory and experiment. *Phys Rev B* 62:7420
- Ogawa T, Takagahara T (1991) Optical absorption and Sommerfeld factors of one-dimensional semiconductors: an exact treatment of excitonic effects. *Phys Rev B* 44:8138
- Phillips RT, Lovering DJ, Denton GJ, Smith GW (1992) Biexciton creation and recombination in a GaAs quantum well. *Phys Rev B* 45:4308
- Ploog K, Döhler GH (1983) Compositional and doping superlattices in III-V semiconductors. *Adv Phys* 32:285
- Pohl UW (2008) InAs/GaAs quantum dots with multimodal size distribution. In: Wang ZM (ed) *Self-assembled quantum dots*. Springer, New York, p 43
- Pope M, Swenberg CE (1982) *Electronic processes in organic crystals*. Oxford University Press, Oxford, UK
- Reynolds DC, Collins TC (1981) *Excitons: their properties and uses*. Academic Press, New York
- Rodina AV, Dietrich M, Göldner A, Eckey L, Hoffmann A, Efros AL, Rosen M, Meyer BK (2001) Free excitons in wurtzite GaN. *Phys Rev B* 64:115204
- Rodt S, Schliwa A, Pötschke K, Guffarth F, Bimberg D (2005) Correlation of structural and few-particle properties of self-organized InAs/GaAs quantum dots. *Phys Rev B* 71:155325
- Rössler U (1979) Fine structure, lineshape, and dispersion of Wannier excitons. In: Treusch J (ed) *Festkörperprobleme. Advances in solid state physics*, vol 19. Vieweg, Braunschweig, p 77
- Rudin S, Reinecke TL, Segall B (1990) Temperature-dependent exciton linewidths in semiconductors. *Phys Rev B* 42:11218
- Scarani V, Bechmann-Pasquucci H, Cerf NJ, Dušek M, Lütkenhaus N, Peev M (2009) The security of practical quantum key distribution. *Rev Mod Phys* 81:1301
- Seguin R, Schliwa A, Rodt S, Pötschke K, Pohl UW, Bimberg D (2005) Size-dependent exciton fine-structure splitting in self-organized InAs/GaAs quantum dots. *Phys Rev Lett* 95:257402
- Shields AJ (2007) Semiconductor quantum light sources. *Nat Photonics* 1:215
- Shields AJ, Pepper M, Ritchie DA, Simmons MY (1995a) Influence of excess electrons and magnetic fields on Mott-Wannier excitons in GaAs quantum wells. *Adv Phys* 44:47
- Shields AJ, Osborne JL, Simmons MY, Pepper M, Ritchie DA (1995b) Magneto-optical spectroscopy of positively charged excitons in GaAs quantum wells. *Phys Rev B* 52:R5523
- Shinada M, Sugano S (1966) Interband optical transitions in extremely anisotropic semiconductors. I. Bound and unbound exciton absorption. *J Phys Soc Jpn* 21:1936
- Shinar J (ed) (2004) *Organic light-emitting devices: a survey*. Springer, New York
- Singh J (1984) The dynamics of excitons. In: Ehrenreich H, Turnbull D (eds) *Solid state physics*, vol 38. p 295, Academic Press, Orlando/New York
- Singh J, Birkedal D, Lyssenko VG, Hvam JM (1996) Binding energy of two-dimensional biexcitons. *Phys Rev B* 53:15909
- Solov'yev VV, Kukushkin IV (2009) Measurement of binding energy of negatively charged excitons in GaAs/Al_{0.3}Ga_{0.7}As quantum wells. *Phys Rev B* 79:233306
- Someya T, Akiyama H, Sakaki H (1996) Enhanced binding energy of one-dimensional excitons in quantum wires. *Phys Rev Lett* 76:2965
- Song KS, Williams RT (1993) *Self-trapped excitons*. Springer series in solid-state sciences, vol 105. Springer, Berlin
- Stébé B, Ainane A (1989) Ground state energy and optical absorption of excitonic trions in two dimensional semiconductors. *Superlattice Microstruct* 5:545
- Tamor MA, Wolfe JP (1980) Drift and diffusion of free excitons in Si. *Phys Rev Lett* 44:1703
- Thewalt MLW, Rostworowski JA (1978) Biexcitons in Si. *Solid State Commun* 25:991
- Thomas GA, Rice TM (1977) Trions, molecules and excitons above the Mott density in Ge. *Solid State Commun* 23:359

- Thomas GA, Timofeev VB (1980) A review of $N = 1$ to ∞ particle complexes in semiconductors. In: Moss TS, Balkanski M (eds) Handbook on semiconductors, vol 2. North Holland Publishing, Amsterdam, p 45
- Tomiki T (1969) Optical constants and exciton states in KCl single crystals III. The spectra of conductivity and of energy loss. *J Phys Soc Jpn* 26:738
- Toyozawa Y (1980) Electrons, holes, and excitons in deformable lattice. In: Kubo R, Hanamura I (eds) Excitons. Springer, Berlin
- Türk V, Rodt S, Stier O, Heitz R, Engelhardt R, Pohl UW, Bimberg D, Steingrüber R (2000) Effect of random field fluctuations on excitonic transitions of individual CdSe quantum dots. *Phys Rev B* 61:9944
- Ueta M, Nishina Y (eds) (1976) Physics of highly excited states in solids. Lecture notes in physics, vol 57. Springer, New York
- Uihlein C, Fröhlich D, Kenklies R (1981) Investigation of exciton fine structure in Cu_2O . *Phys Rev B* 23:2731
- Vogl P (1976) Microscopic theory of electron-phonon interaction in insulators or semiconductors. *Phys Rev B* 13:694
- Vouilloz F, Oberli DY, Dupertuis M-A, Gustafsson A, Reinhardt F, Kapon E (1997) Polarization anisotropy and valence band mixing in semiconductor quantum wires. *Phys Rev Lett* 78:1580
- Vouilloz F, Oberli DY, Dupertuis M-A, Gustafsson A, Reinhardt F, Kapon E (1998) Effect of lateral confinement on valence-band mixing and polarization anisotropy in quantum wires. *Phys Rev B* 57:12378
- Wang X-L, Voliotis V (2006) Epitaxial growth and optical properties of semiconductor quantum wires. *J Appl Phys* 99:121301
- Wannier GH (1937) The structure of electronic excitation levels in insulating crystals. *Phys Rev* 52:191
- Washington MA, Genack AZ, Cummins HZ, Bruce RH, Compaan A, Forman RA (1977) Spectroscopy of excited yellow exciton states in Cu_2O by forbidden resonant Raman scattering. *Phys Rev B* 15:2145
- Weisbuch C, Benisty H, Houdré R (2000) Overview of fundamentals and applications of electrons, excitons and photons in confined structures. *J Lumin* 85:271
- Wicksted J, Matsushita M, Cummins HZ, Shigenari T, Lu XZ (1984) Resonant Brillouin scattering in CdS. I. Experiment. *Phys Rev B* 29:3350
- Yamada Y, Sakashita T, Watanabe H, Kugimiya H, Nakamura S, Taguchi T (2000) Optical properties of biexcitons in ZnS. *Phys Rev B* 61:8363
- Yu PY (1979) Study of excitons and exciton-phonon interactions by resonant Raman and Brillouin spectroscopies. In: Cho K (ed) Excitons. Springer, Berlin, p 211
- Yu PW, Reynolds DC, Bajaj KK, Litton CW, Klem J, Huang D, Morkoc H (1987) Observation of monolayer fluctuations in the excited states of $\text{GaAs-Al}_x\text{Ga}_{1-x}\text{As}$ multiple-quantum-well. *Solid State Commun* 62:41
- Zieliński M, Gołasa K, Molas MR, Goryca M, Kazimierzuk T, Smoleński T, Golnik A, Kossacki P, Nicolet AAL, Potemski M, Wasilewski ZR, Babiński A (2015) Excitonic complexes in natural InAs/GaAs quantum dots. *Phys Rev B* 91:085303